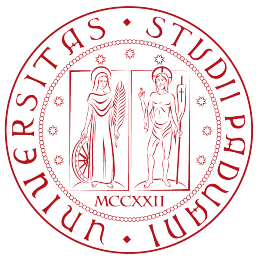

UNIVERSITÀ DEGLI STUDI DI PADOVA

Dipartimento di Fisica e Astronomia "Galileo Galilei"

Dipartimento di Matematica "Tullio Levi-Civita"

Corso di Laurea Magistrale in Fisica

Tesi di Laurea

Modeling how CaV channel motion in the cell membrane affects formation of the BK_{Ca}-CaV complex

Relatore

Prof. Marco Ferrante

Correlatore

Prof. Morten Gram Pedersen

Laureando

Eleonora Martini

Anno Accademico 2018/2019

Contents

Introduction

The main purpose of the thesis is to better understand the interaction between large-conductance Ca^{2+}-dependent K^+ (BK_{Ca}) channels and voltage-gated Ca^{2+} (CaV) channels. It has been observed, in neurons and vascular myocytes, that these channels colocalize and form ion channel complexes $BK_{Ca}-CaV$. This configuration exposes the BK_{Ca} channel to a direct influx of Ca^{2+} everytime the bonded CaV channel opens. Stochastic simulations of the complex activity offer significant insight into the local control of BK_{Ca} channels by fluctuating nanodomains of Ca^{2+}, but on the other hand such Monte Carlo simulations are computationally expensive.
The starting point of the study is a model for the $BK_{Ca}-CaV$ presented in [1], whose aim is to analyze the complex using Markov chain theory. The crucial step of this work is the derivation, from the description of a single $BK_{Ca}-CaV$ complex, of a concise model of whole-cell BK_{Ca} currents. This model offer a simple formulation of these whole-cell currents that respects local interactions in the complex and also suggests how local-global coupling of ion channels are able to influence cell behavior.
As reported in [2] and [3], molecular research has shown that the activity of ion channels is not only determined by the pore forming α-subunits, but it is deeply influenced by the molecular environment. There is evidence that many membrane proteins associate with partner proteins or even colocalize and form complexes. These complexes exhibit different behaviors depending on the properties of the molecules involved. Association of proteins may modulate channel function, affect downstream signaling pathways, or shape spatio-temporal concentration gradients of ions or diffusible messengers.
K_Ca channels are responsible for a variety of cellular processes and most of their functions are brought about by interaction of the channels' pore-forming subunits with distinct partner proteins. These channels are activated by an increase in Ca^{2+} internal concentration and their action feeds back onto $[Ca^{2+}]_i$. The opening of K_Ca channels causes a repolarization of the membrane potential which initiates the deactivation of the CaV channels, thus limiting Ca^{2+} influx.
The crucial role of BK_{Ca} channels in membrane hyperpolarization in response to an increased level of $[Ca^{2+}]_i$ is critically dependent on their integration into complexes with other proteins. The stable association with partner proteins is used to optimally adapt the channels to their distinct and cell type-specific physiological functions. We consider in particular BK_{Ca} channels, that exhibit large conductance unitary and are gated by the cooperative action of membrane depolarization and $[Ca^{2+}]_i$. Under cellular conditions, both stimuli contribute in a concerted way to BK channels activity, and in the physiological voltage range considerable activation is observed for $[Ca^{2+}]_i \geq 10\ \mu M$. The Ca^{2+} ions are supplied by the opening of CaV channels and the level of concentration required to activate the BK is thought to be available only in the immediate proximity of the sources: this implies close colocalization of BK_{Ca} and CaV channels, which can be considered as a direct channel-channel interaction. Experimental results on molecular masses suggest $1:4$ stoichiometry and pore-to-pore distance $\sim 10\ nm$. Among the advantages of this kind of interaction is that consistent activation of BK_{Ca} is guaranteed in the physiological voltage range and even in the presence of highly active Ca^{2+} buffering system.

Thanks the formation of the complex, BK_{Ca} activation is managed locally, as the required concentration of Ca^{2+} ions is guaranteed in the vicinity of the BK_{Ca} and there is virtually no dependence on the global cellular Ca^{2+} environment.
As we said, the model devised in [1] is centered on the activity of the $BK_{Ca} - CaV$ complex, meaning the two channels are considered while they interact at a fixed distance that is the distance typical of the bond. The contribution provided by our work is the analysis of the dynamics that may bring to the complex formation: in other words, in an attempt to construct a more realistic model, we introduce the CaV channel Brownian motion in the cell membrane and we study how this aspect influence the activity of the BK_{Ca}. More specifically we investigate what is the probability of complex formation given the properties of channel diffusion in the membrane, and we characterize the interaction of the BK_{Ca} channel with the CaV channels when they are not bonded in the complex.
The first chapter offer an overview of [1], in order to introduce the dynamics of the channels and the kind of analysis that we are going to extend with the inclusion of the CaV Brownian motion in the next chapters. In fact in chapter 2 we start performing a Monte Carlo simulation of the CaV diffusion around the BK_{Ca} and we focus on the probability of complex formation and on its contribution to the BK_{Ca} channel open probability. Then in chapter 3 we use the results of the previous Monte Carlo simulation to model the CaV channel diffusion on a grid, for which it is possible to define a Markov chain. Considering this Markov chain, first we realize a new Monte Carlo simulation, and after that we derive a system of ordinary differential equations for the time evolution of the probabilities of the Markov chain.

Chapter 1

Modeling of BK_{Ca}-CaV activity

1.1 Model for the BK_{Ca} channel

We describe the BK channel as having two states, closed (X) and open (Y). The activation probability of the channel is governed by the differential equation:

$$\frac{dp_Y}{dt} = -k^- p_Y + k^+(1 - p_Y). \tag{1.1}$$

The rate constants k^+ and k^- depend on both the membrane voltage and the Ca_{2+} concentration, denoted as Ca in the equations below, as we can see from their expressions:

$$\begin{aligned} k^- &= w^-(V)f^(Ca) \\ k^+ &= w^+(V)f^+(ca). \end{aligned} \tag{1.2}$$

For the voltage-dependent rate constants the following standard form is assumed:

$$\begin{aligned} w^-(V) &= w_0^- \exp(-w_{yx}V) \\ w^+(V) &= w_0^+ \exp(-w_{xy}V) \end{aligned} \tag{1.3}$$

because at fixed Ca_{2+} levels the channel activation is well described by Boltzmann functions. On the other hand, there is evidence that at fixed voltage the calcium dependance is given by the relations:

$$\begin{aligned} f^-(Ca) = 1 - \frac{Ca^{n_{yx}}}{K_{yx}^{n_{yx}} + Ca^{n_{yx}}} &= \frac{1}{1 + \left(\frac{Ca}{K_{yx}}\right)^{n_{yx}}} \\ f^+(Ca) = \frac{Ca^{n_{xy}}}{K_{xy}^{n_{xy}} + Ca^{n_{xy}}} &= \frac{1}{1 + \left(\frac{K_{yx}}{Ca}\right)^{n_{xy}}} \end{aligned} \tag{1.4}$$

where K_{yx} and K_{xy} are the calcium affinities when the channel closes and opens, respectively, and n_{yx} and n_{xy} are the corresponding Hill coefficients.
Using the relationships above it is possible to write formulas for the equilibrium open fraction of BK channels, $p_{Y\infty}$ and the related time constant τ_{p_Y}:

$$\begin{aligned} p_{Y\infty} &= \frac{k^+}{k^- + k^+} \\ \tau_{p_Y} &= \frac{1}{k^- + k^+}. \end{aligned} \tag{1.5}$$

w_0^-	$3.32\ ms^{-1}$
w_0^+	$1.11\ ms^{-1}$
w_{yx}	$0.022\ mV^{-1}$
w_{xy}	$-0.036\ mV^{-1}$
K_{yx}	$0.1\ \mu M$
K_{xy}	$16.6\ \mu M$
n_{yx}	0.46
n_{xy}	2.33

Table 1.1: *Parameters used in the BK_{Ca} channel model*

Through global optimization it was possible to estimate the model parameters providing the best fit to the experimental data from [4]. These parameters are shown in table 1.1 and they will be used in the model that we are going to implement in the next chapters.

We have said that k^- and k^+ depend on the Ca_{2+} concentration, and now we want to better define this dependance. More specifically, in fact, these rates are determined by the Ca_{2+} concentration that is perceived by the related sensor of the BK channel. When the CaV channel are closed, only the background concentrations of Ca_{2+} ions, which is set equal to 0.2 μM, is present. Putting this value into the expression for k^+ we obtain that the rate is virtually zero, therefore it is not possible to observe BK activation induced only by the background concentration.
On the other hand, when a CaV is open, the potassium channel will react to the increased concentration of Ca_{2+} ions on the basis of the distance at which the CaV is located. The precise value of the Ca_{2+} concentration perceived by the BK in this case is given by the formula:

$$Ca_o = \frac{i_{Ca}}{8\pi r D_{Ca} F} exp\left(\frac{-r}{\sqrt{\frac{D_{Ca}}{k_B^+[B_{total}]}}}\right). \tag{1.6}$$

where $i_{Ca} = g_{Ca}(V - V_{Ca})$ is the single channel current. The parameters in table 1.2 are taken from [4].
This model considers the BK_{Ca}-CaV complex, meaning the BK activation is studied in the case when the CaV is bonded to the BK. Under this conditions the distance between the two channels is 13 nm and this distance is used to calculate Ca_o in order to obtain the value of the activation rate when the CaV is open.

r	$13\ nm$
D_{Ca}	$250\ \mu m^2 s^{-1}$
F	$9.6485\ Cmol^{-1}$
k_B	$500\ \mu M^{-1} s^{-1}$
B_{total}	$30\ \mu M$
V_Ca	$60\ mV$
g_{Ca}	$2.8\ pS$

Table 1.2: *Parameters used to calculate the Ca^{2+} concentration as function of the distance from the source*

1.2 Model for the CaV channel

The CaV dynamics is described by the following equations:

$$\begin{aligned} \frac{dc}{dt} &= \beta o - \alpha c \\ \frac{do}{dt} &= \alpha c + \gamma b - (\beta + \delta) o \\ b &= 1 - c - o = 1 - h \end{aligned} \tag{1.7}$$

where c indicates the closed state, o indicates the open state and b indicates the inactivated (or blocked) state of the channel. Then h represents the fraction of calcium channels that are not inactivated. Correspondently, α is the opening rate, β is the closing rate, δ is the inactivation rate and γ is the reactivation rate. The dynamics between the open and the closed state is determined by the voltage of the membrane and the expressions for α and β are:

$$\begin{aligned} \alpha(V) &= \alpha_0 \exp(-\alpha_1 V) \\ \beta(V) &= \rho \left(\beta_0 \exp(-\beta_1 V) + \alpha_0 \exp(-\alpha_1 V)\right). \end{aligned} \tag{1.8}$$

The inactivated state is not the same as the closed state, in the sense that it corresponds to a different configuration of the ion channel. The process of inactivation is driven by the Ca_{2+} concentration, thus the expression for the rates is given by:

$$\begin{aligned} \delta &= 0.0025\ \mu M^{-1} \cdot [Ca_{CaV}] \\ \gamma &= 0.0020\ ms^{-1} \end{aligned} \tag{1.9}$$

where Ca_{CaV} is the concentration at the internal mouth of the channel and can be calculated through equation 1.1 setting $r = 7\ nm$, that is the distance of the sensor for Ca_{2+}-dependent inactivation from the channel pore. Both the rates in equation 1.2 are taken from Cox.
It has been shown by Sherman that the dynamics of channel activation is considerably faster than inactivation (and subsequent re-activation), therefore the two processes can be approximately separated in time. As a consequence, it is possible to devise a model for the so-called activation variable of the calcium channel

$$\frac{dm_{CaV}}{dt} = \frac{m_{CaV\infty} - m_{CaV}}{\tau_{CaV}} \tag{1.10}$$

where

$$\begin{aligned} m_{CaV\infty} &= \frac{\alpha}{\alpha + \beta} \\ \tau_{CaV} &= \frac{1}{\alpha + \beta} \end{aligned} \tag{1.11}$$

and to write an equation for the fraction of inactivated CaV channels:

$$\frac{db}{dt} = m_{CaV\infty}\delta - (m_{CaV\infty}\delta + \gamma) b. \tag{1.12}$$

Also in the case of the calcium channel global optimization was used to identify the best set of parameters for the activation model. These parameters are reported in table 1.3 below, and they will be used throughout this work everytime we will treat CaV activation.

α_0	$1.324\ ms^{-1}$
α_1	$-0.0487\ mV^{-1}$
β_0	$0.165\ ms^{-1}$
β_1	$0.1735\ mV^{-1}$
ρ	0.384

Table 1.3: *Parameters used in the CaV channel model*

1.3 Markov chain model of the BK_{Ca}-CaV complex

Combining the three-state model for the CaV and the two-state model for the BK described in the previous sections, the authors in [1] define a six-state Markov chain model for the complex, that is illustrated in figure 1.1. For this Markov chain it is immediate to write two matrices of

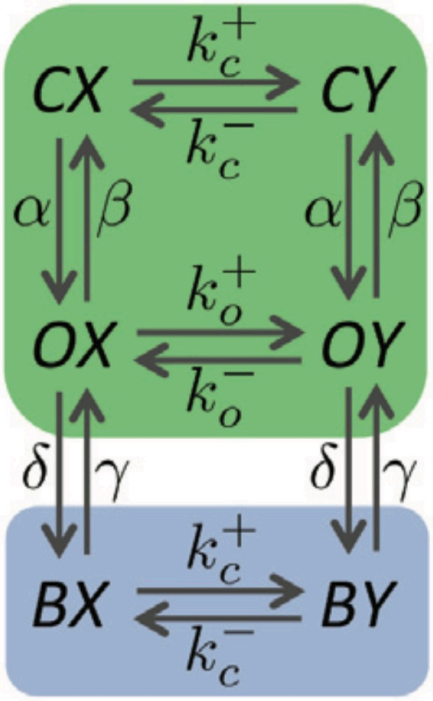

Figure 1.1:

transition probabilities, one for the dynamics of the calcium channel and one for the activity of the BK, that is determined at every instant on the basis of the CaV state. Using these matrices, Monte Carlo simulations are performed in order to study the stochastic gating of the BK_{Ca}-CaV complex. The results of the simulations are shown below in figure 1.3.
Since the model has a manageable number of states, and besides rate $k_c^+ \approx 0$, it is possible to compute explicit formulas for the average time to first opening of the potassium channel, meaning the first time the Markov chain visit one of the states CY, OY or BY starting from CX, and for the distribution function $P(T_{CX} < t)$, that represents the probability of BK opening before a given time t. The authors found:

$$\begin{aligned} E(T_{CX,Y}) &= \frac{1}{\alpha} + \frac{1}{k_o^+} + \frac{1}{k_o^+}\left(\frac{\beta}{\alpha} + \frac{\delta}{\gamma}\right) \\ P(T_{CX,Y} < t) &= 1 - \sum_{\psi \in \{C,O,B\}} (exp(tQ))_{CX,\psi X} \end{aligned} \tag{1.13}$$

using phase-type distribution results for Markov chains. Q is the subtransitions rate matrix of the Markov chain corresponding to states $\{CX, OX, BX\}$.
The biphasic behaviour shown in figure 1.2, taken from [1], is the result of the combination of the two processes with different time scales, activation and inactivation of the CaV channel.

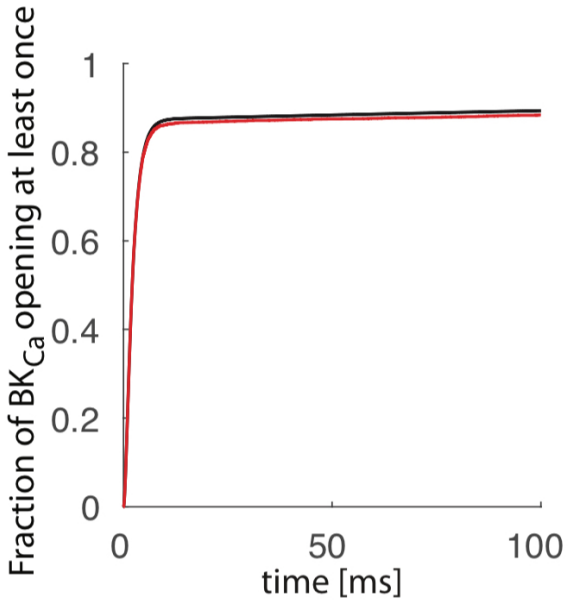

Figure 1.2: *Comparison between the empirical fraction of BK channels which show the first opening before t (red) and the theoretical expression in equation 1.13 (black). Figures are taken from [1].*

1.4 Deterministic model of cellular BK$_{Ca}$ activity

The aim of this model is to find the evolution over time of the BK open probability p_Y, so that it is possible to evaluate the whole-cell current $I_{BK} = g_{BK} p_Y (V - V_K)$, where g_{BK} is the maximal whole-cell BK conductance and V_K is the K^+ reversal potential.
The time evolution of the probability distribution of the six-state Markov chain can be described by a system of five ordinary differential equations, because the probabilities sum to 1. The BK open probability can be calculated as $p_Y(t) = p_{CY}(t) + p_{OY}(t) + p_{BY}(t)$.
In order to obtain an expression for the BK current of Hodgkin-Huxley form, the system of 5 ODEs is reduced through detailed time-scale analysis. In fact, since inactivation and re-activation of the CaV are slower processes than activation and de-activation, if a fast time-scale is considered it is possible to assume that the average fraction of non-inactivated calcium channel, $h = 1 - p_{BX} - p_{BY}$, is constant. This assumption corresponds to separating the model in two sub-models with four and two states, respectively the green box and the blue box in figure 1.1. So now it is necessary to manipulate the reduced system of ODEs which describes the four-state sub-model with non-inactivated CaVs. Analysing the dependance on voltage of the transitions rates, one sees that the dynamics of the CY state is the fastest, so its probability can be considered in a quasi-steady state. At this point one is left with a single differential

equation for the BK activation variable m_{BK}:

$$\begin{aligned} \frac{dm_{BK}}{dt} &= \frac{m_{BK\infty} - m_{BK}}{\tau_{BK}} \\ m_{BK\infty} &= \frac{m_{CaV} k_o^+ (\alpha + \beta + k_c^-)}{(k_o^+ + k_o^-)(k_c^- + \alpha) + \beta k_c^-} \\ \tau_{BK} &= \frac{\alpha + \beta + k_c^-}{(k_o^+ + k_o^-)(k_c^- + \alpha) + \beta k_c^-}. \end{aligned} \tag{1.14}$$

Since BK channels close rapidly in complexes with inactivated CaVs, it is possible to write $p_Y \approx m_{BK} h$, so that the BK current is approximated by the standard Hodgkin-Huxley ([5]) espression

$$I_{BK} = g_{BK} m_{BK} h (V - V_K). \tag{1.15}$$

Figure 1.3 shows the comparison between the method illustrated so far. In the first plot we can see the CaV open probabilities in response to a voltage step from -80 to 0 mV, while the second plot represents the BK open probability in response to the same voltage step. We notice in particular that the simplyfied Hodgkin-Huxley-type model approximates very well the results given by the Monte Carlo simulation and the complete ODE system.
The point of reaching this kind of expression for the BK current is that it can be inserted in whole-cell models of different types of excitable cells.
The plots in figure 1.4 are the steady-state for the BK activation variable and its time constant (the light-blue lines represent the case with one CaV).

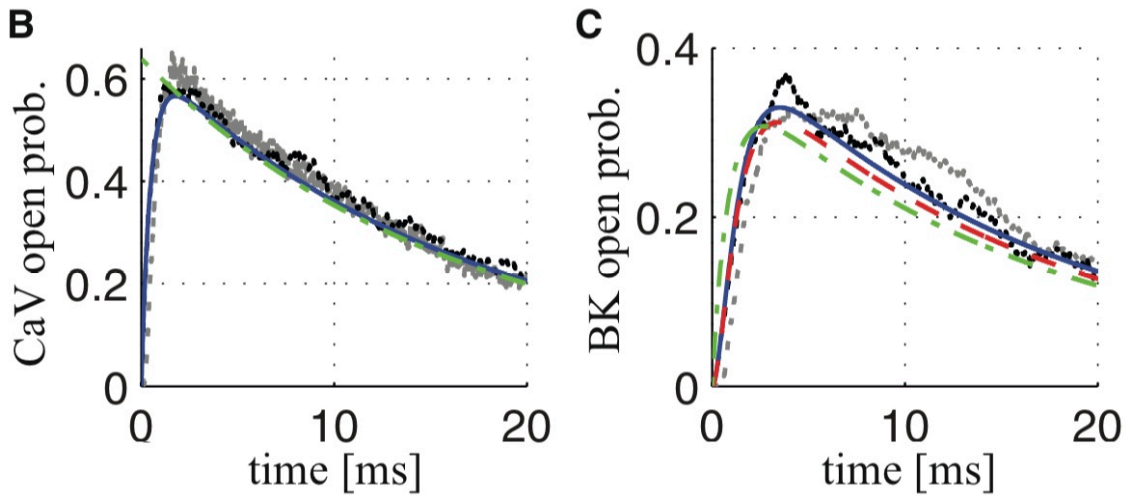

Figure 1.3: *CaV and BK open probabilities, comparison between different methods. Figures are taken from [1]. In particular in box C we can see: the* 70*-state Markov chain model presented in [4] (grey), the six-state Markov chain model (black), the ODE model corresponding to the six-state model (blue), the simplified Hodgkin-Huxley-type model expressed by the equation above for* I_{BK} *(dashed red).*

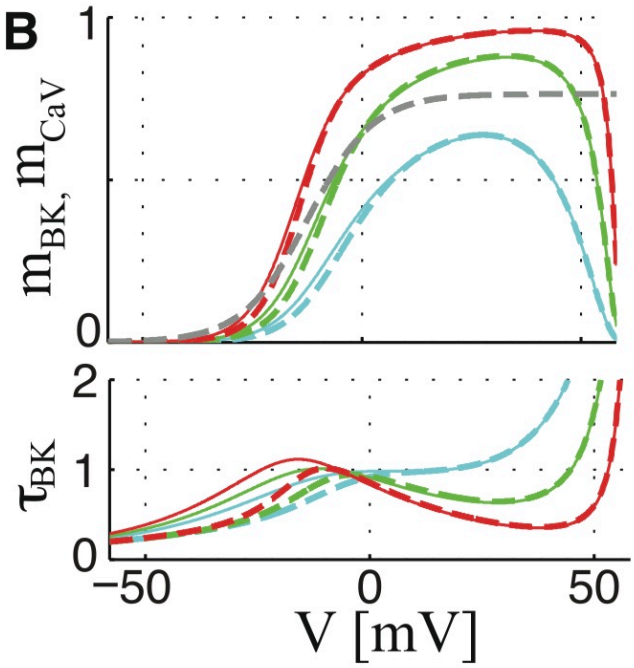

Figure 1.4: *Steady-state BK activation function (upper) and time constant (lower) for BK channels in complexes with 1 (cyan), 2 (green) or 3 (red). The grey dashed curve shows the CaV steady-state activation function. Figure taken from [1].*

Chapter 2

Analysis of CaV Brownian motion and complex formation

2.1 Introducing CaV diffusion

Our aim is to understand how local interaction between BK channels and the surrounding CaV channels influences the BK activity. The first part of this work provides a Monte Carlo simulation of calcium channels Brownian motion in the cell membrane. We want to study a portion of the membrane where only one BK is present and the area of this portion will be set out starting from the BK channels numerical density, that can be different depending on the type of cell examinated.
As benchmark we consider neurons: the source for the channel densities is [6], which gives $n_{BK} \simeq 18\ \mu m^{-2}$. Thus the mean distance between two adiacent BKs will then be $r_{mean} \simeq 1/\sqrt{18}\ \mu m = 0.2357\ \mu m$, and the diffusion will be simulated in a circular area of radius $r_{max} = r_{mean}/2 = 0.11785\ \mu m$. The mean number of CaVs that are contained in this area is calculated using the CaVs numerical density $n_{CaV} \simeq 100\ \mu m^{-2}$ ([6]), and we find that on average there are $n_{CaV}\pi r_{max}^2 = 4.3$ calcium channels within a distance r_{max} from every BK.
We choose to consider a circular area around the BK, instead of the slightly larger square area obtained immediately from the inverse of the BK channels density, because our problem presents radial symmetry, since the parameter of interest is the distance between the BK and the CaVs. This configuration happens to be more practical to perform the simulation and, in particular, it will enable us to define a series of shells around the BK, that will be used to implement the grid of our discrete model. At the end of this section, in the discussion of the results of the simulation, it will be clear that using a circular area does not affect the consistency of the model: in fact, the calcium channels that we are neglecting are located in what we will call the dead zone, meaning that the BK is not able to perceive the presence of the CaVs in those regions because they are too distant.
Assuming that this portion of the membrane is homogeneous, we expect that the kind of mobility the CaVs exhibit is simple Brownian translational diffusion in the plane of the membrane and we describe it as a random walk. An estimate of the distance travelled by the diffusing particle during a certain time interval is given by the square root of its mean squared displacement over that interval. Specifically, in the case of a two-dimensional random walk, the theory of Brownian motion provides us with the relation

$$MSD(n\tau) = 4Dn\tau \tag{2.1}$$

where D is the diffusion coefficient, τ is the time step of the random walk, meaning the inverse of the frequency at which the particle position is sampled, n is the number of time steps that are considered and thus $n\tau$ is the time interval over which the particle is observed. Eq. 2.1 highlights the fact that for a pure Brownian motion the diffusion coefficient is independent of the sampling frequency or the total time interval.
However, calcium channels happen to encounter and transiently bind to the BK while diffusing in the membrane, so their motion is not strictly free. The mode of mobility which describes more properly our system is therefore transient anchorage ([7]), that is a combination of free Brownian motion and strongly confined diffusion around the anchorage points. The center of our analysis is indeed the formation of the BK_{Ca}-CaV complex, and we need to model it in such a way that makes it possible to include it in the CaV channel trajectories. We know from [4] that when the BK and the CaV are bonded they are located 13 nm apart. We then represent the anchorage as an area of radius $r_{min} = 13\ nm$ around the BK where the calcium channels, once they enter it, perform a Brownian motion characterised by a different, namely smaller, diffusion coefficient, which indicates the fact that their mobility is reduced by the bond.
The values for the two diffusion coefficients that will be used in the model are taken from [8]:

$$\begin{aligned} D_{free} &= 0.035\ \mu m^2/s \\ D_{complex} &= 0.007\ \mu m^2/s \end{aligned} \tag{2.2}$$

To sum up, the channel trajectories that we simulate are given by the combination of two free Brownian motion with different diffusion coefficients, so we are not treating a pure Brownian diffusion and it is not possible to apply equation 2.1 straightforwardly. It is necessary to find out what the relationship between MSD and time is in this case and, even more important, how a variation of the time step affects the CaV trajectories. In particular, we need to understand in what way the choice of the sampling frequency influences the probability of complex formation and how it may reflect on the BK dynamics. It is clear that defining the right τ is crucial to ensure the consistency of the model.

2.2 Monte Carlo simulation of CaV Brownian motion and choice of the time step

In this section we discuss the features of the Brownian motion simulation and present an overview of the results.
Figure 2.1 shows the area considered to simulate calcium channels diffusion. The initial positions of the channels will be distributed uniformly in the shell limited by r_{max} and r_{min}, thus at time zero there will be no complex. Since we suppose that the system is homogeneous, the number of CaVs that can be find at distance $\leq r_{max}$ is constant and, as we saw above, it can be deduced from the channels numerical density. This means that, for every CaV which goes beyond the maximum distance, there will be another one which enters the area. To implement this aspect, reflecting boundary conditions are used, so that the trajectories appear continuous: every time a channel exits the region delimited by the outer circle the next displacement will be set as the opposite of the previous one, basically bringing the channel back at its last position inside the area. In the simulation of the channel dynamics between its states that will be carried out afterwards, we will set $\tau_{dynamics} = 0.01\ ms$ ([1]). Adopting the same time step for the simulation of Brownian motion would certainly be correct, but it would also entail significant computational cost. Since the channel diffusion and the transitions between its states are independent processes, it is possible to use different time steps. Starting from the assumption that the smaller the τ, the better the random walk can approximate Brownian

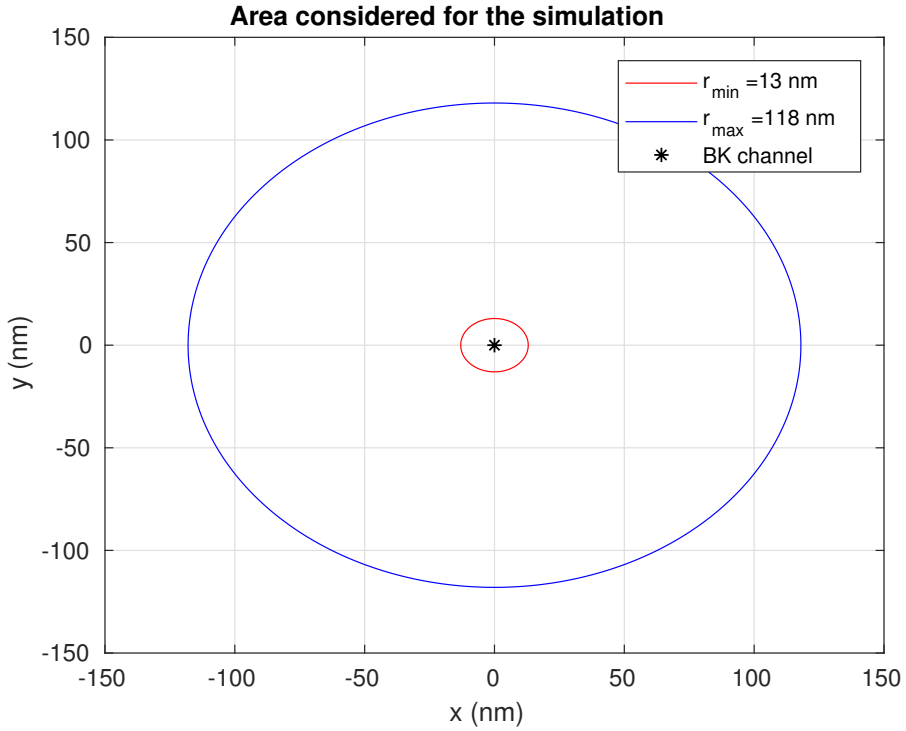

Figure 2.1: *Scheme of the area defined around a single BK to simulate the calcium channels diffusion.*

motion, we are looking for an upper limit for the sampling time, a value which allows us to get a manageable Monte Carlo simulation without introducing any bias on the BK dynamics. We proceed analysing the details of CaVs diffusion in order to identify an interval of acceptable time steps.

We sample the channel trajectories for 100 ms and we find that, as it was expected, the relationship between MSD and time is not linear, due to the contribution of the two different diffusion coefficients.

In order to understand the dependance of the trajectory on the time step, we compare the mean value of MSD in time for different τ. As it is can be seen in figure 2.2, the lines practically overlap for short times, and then begin to separate as time increases, because the trajectories sampled at lower frequency present larger values of MSD. Considering that the channel dynamics will be simulated for 50 ms ([1]), on the basis of figure 2.2 we can say that good values for τ are contained in the interval $[0.01, 0.1]$ ms, for these sampling frequencies give approximately the same description of the channel motion. For a more quantitative analysis, we check that the BK dynamics is left unchanged when the diffusion time step is taken within this range. As first indicator we consider the probability to find that at least one CaV channel is bonded to the BK, which is shown in figure 2.3 as function of the sampling time. The variation of the probability over the interval $[0.01, 0.1]$ ms is negligible, since it concerns the second decimal place, but it becomes more consistent when τ is brought to 0.5 ms.

The fact that the probability to observe the BK_{Ca}-CaV complex remains practically constant over the considered range of time steps can be deduced also from figure 2.4: in fact, the plots show that, as τ increases, the single-channel residence time in the complex becomes longer, but the number of times the CaV bonds with the BK decreases correspondingly.

To get the validation that $[0.01, 0.1]$ ms is a good range for the sampling time, we try and see how different values of τ affect the BK open probability, which is the quantity at the heart of this work. It is interesting to note in 2.5 that the BK open probability in time is practically the same for the smaller values of τ in the range, but as the time step increases beyond 0.1 ms it becomes smaller. An explanation of this decline can be that, as it is reported in [1], the

time constant for the BK opening at 0 mV is just about 0.5 ms, so sampling the Brownian diffusion at this same frequency results in a variation of the opening probability. Besides, we see in figures 2.6 and 2.7 that for $\tau = 0.5$ ms the contribution to the BK open probability given by the CaV channels which are in the complex is reduced. This appears to be the consequence of the decline in the probability to find the complex that is highlighted in figure 2.3.
Since the main purpose of this work, as already reminded, is to better estimate the BK opening probability and to understand the role of the complex formation in the BK activity, it is crucial to set a time step that leads to a correct evaluation of these features of the system. Hence it is possible to conclude that, in the context of the problem we are studying, setting a time step of 0.1 ms allows us to speed up the Monte Carlo simulation and also ensures the consistency of the model.

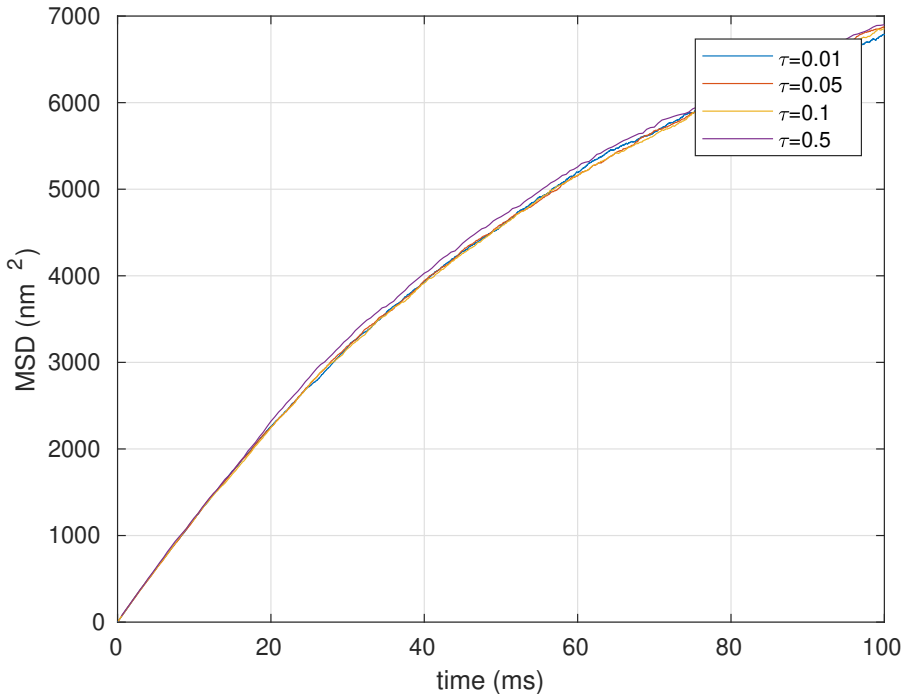

Figure 2.2: *Comparison between the mean squared displacement of trajectories simulated with different sampling frequencies.*

2.3 Effects of CaV diffusion on complex formation and BK open probability

Now we proceed discussing the meaning of the plots obtained for the BK open probability in time.
First we consider the case where only one CaV is present. Figure 2.8 shows that, as it was predictable, introducing the calcium channel diffusion lowers the probability of BK activation, compared to the case where the calcium channel is fixed at the bond distance ([1]), because the BK channel can perceive only partially or even not at all the increased Ca^{2+} concentration when the open Cav channel is located farther than 13 nm.
However, what is worth noticing in figure 2.8 is the fact that the BK_{Ca}-CaV complex accounts for only half of the BK open probability, meaning the CaVs which are not bonded to the potassium channel contribute to its activation to the same extent as the ones that form the complex. This result was not to be assumed and it requires further investigation on the conditions which

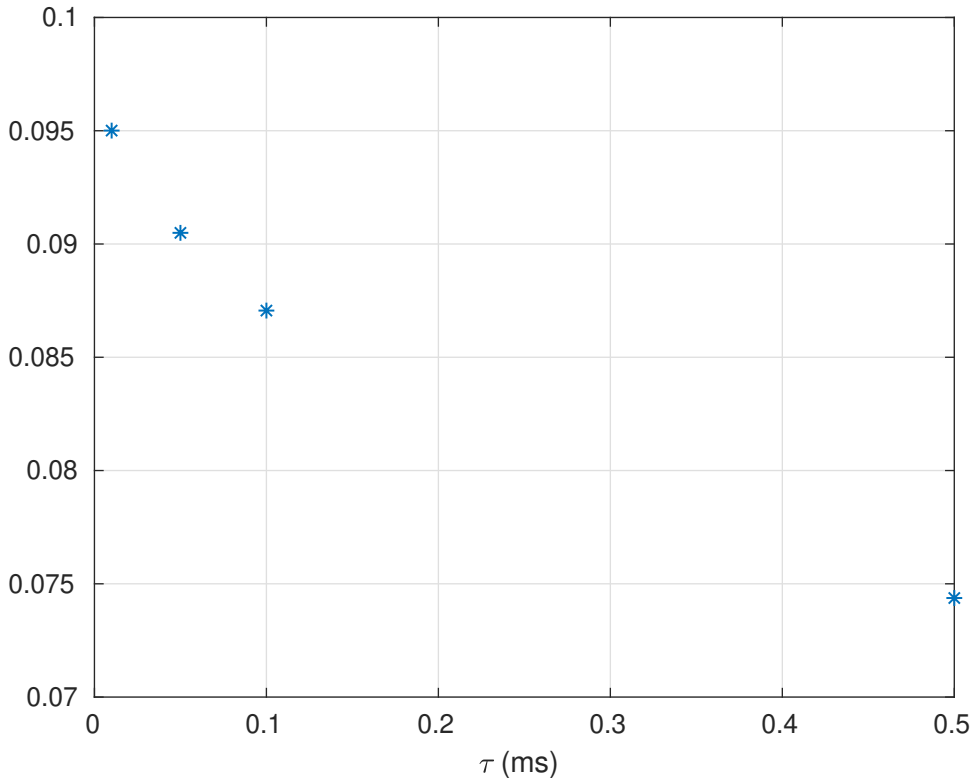

Figure 2.3: *Probability to observe the BK_{Ca}-CaV complex as function of the sampling time, when only one calcium channel is present.*

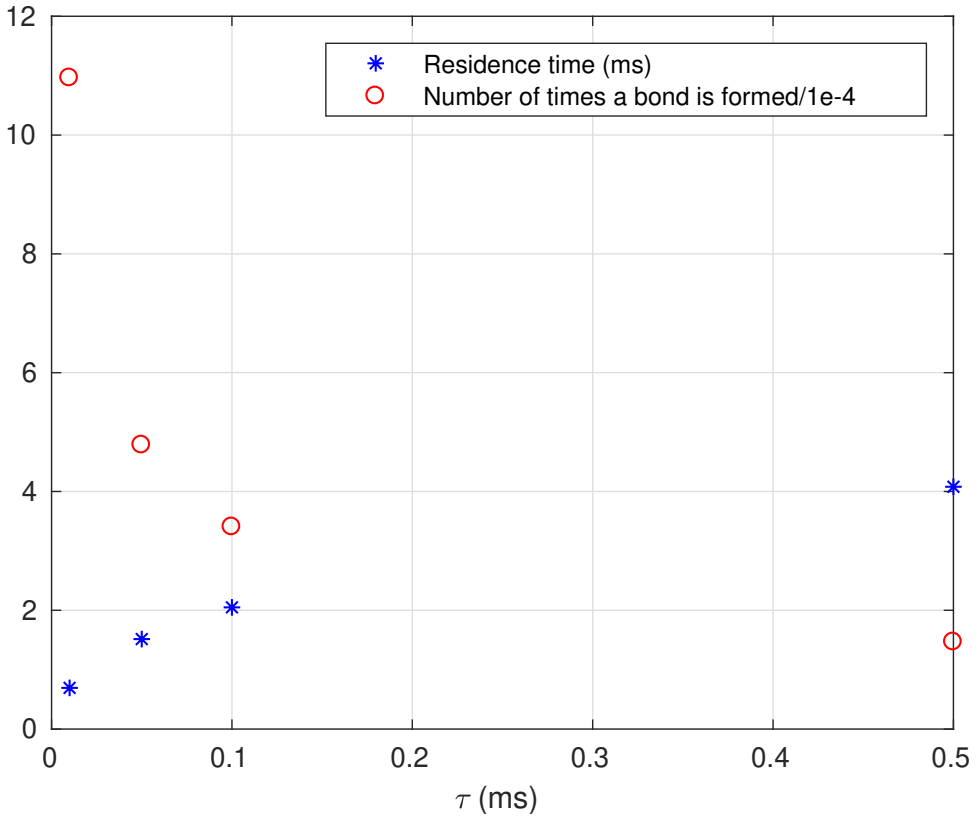

Figure 2.4: *Single-channel residence time in the BK_{Ca}-CaV complex as function of the sampling time. The red circles indicate the corresponding number of times the calcium channel bonds with the BK, divided by 10^4.*

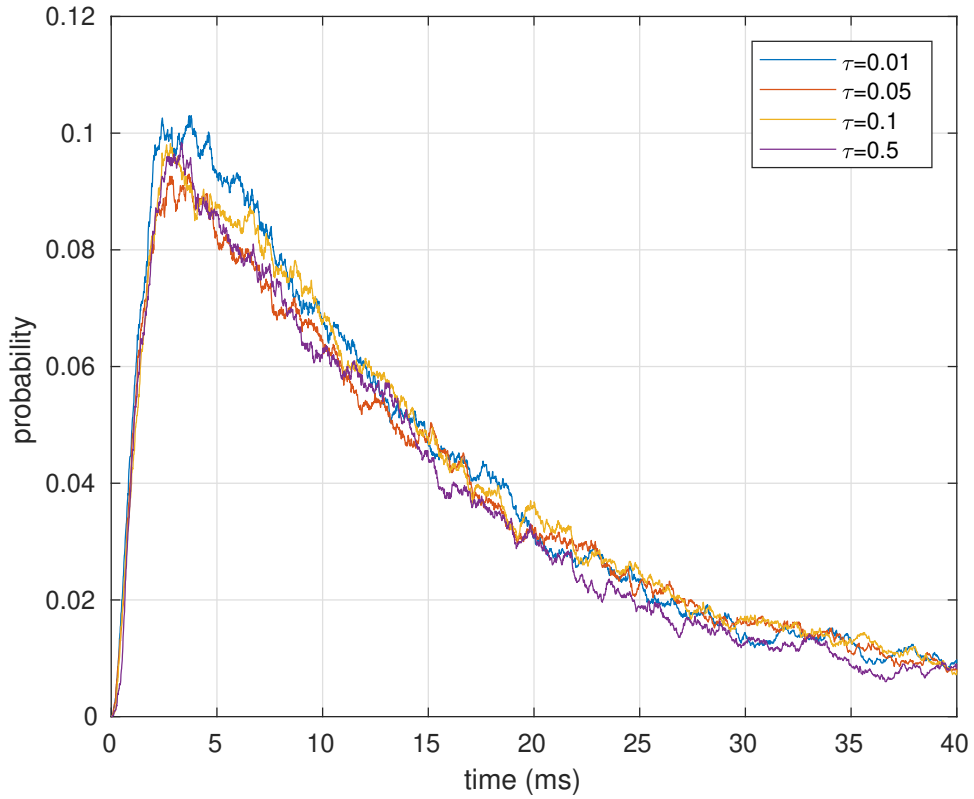

Figure 2.5: *BK open probability calculated using different sampling time for the CaV diffusion.*

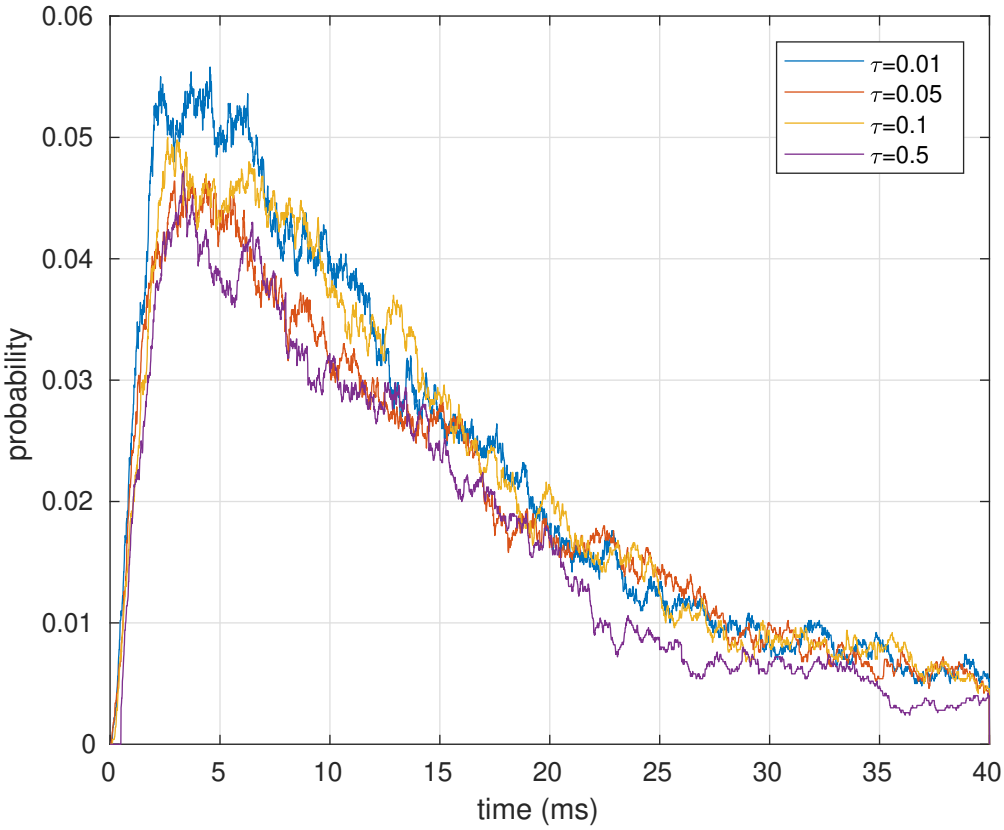

Figure 2.6: *BK_{Ca}-CaV complex contribution to BK opening probability, calculated from the simulation of one calcium channel diffusion with different sampling time. The case with $\tau = 0.5$ ms, represented by the violet line, appears to be lower in comparison with smaller time steps and this tendency may affect the results on the role of the complex in the BK activation.*

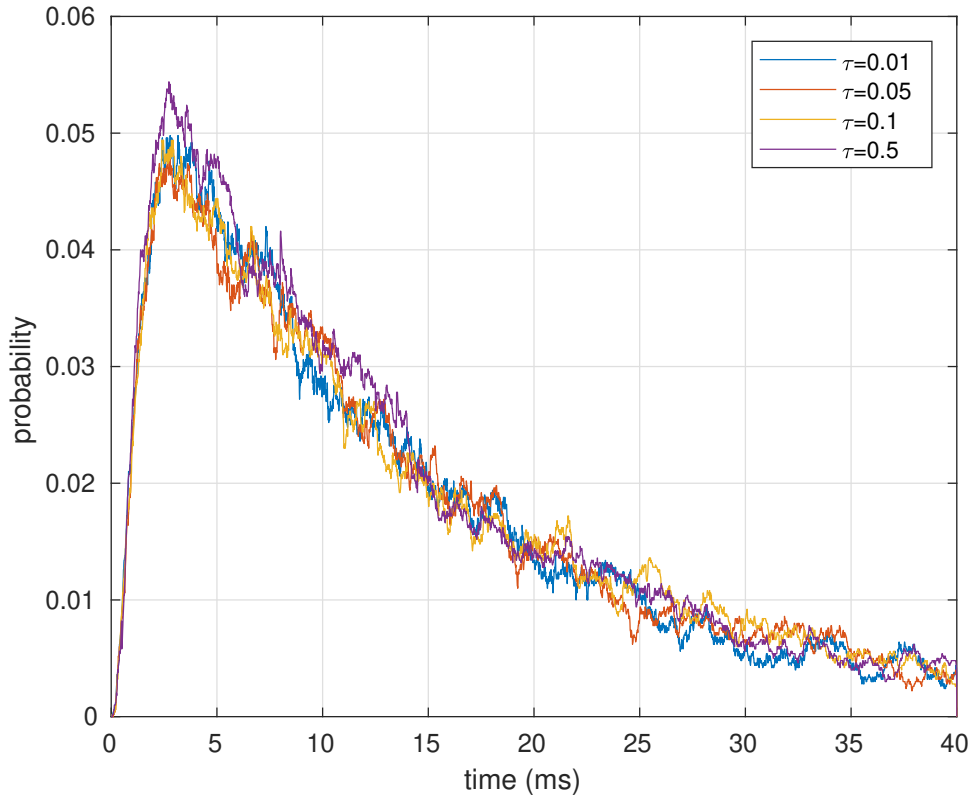

Figure 2.7: *Probability of BK opening without complex formation, calculated from the simulation of one calcium channel diffusion with different sampling time.*

activate the BK.

To get an idea of how the distance between the CaV and the BK influences the dynamics of the latter, we divide the area in figure 2.1 in three shells: the first one represents the complex and its limit is set at $r_{min} = 13\ nm$; the second one is between 13 nm and $3r_{min} = 39\ nm$ and it is the area that will be considered in the discrete model; the third shell is the remaining area between 39 nm and the boundary. The purpose is to estimate in what measure the open calcium channels that are located in each shell are responsible for the BK opening.

The most accurate information on the distribution of the active calcium channel is given by the cumulative probability in figure 2.9. We observe that the function rises steeply, reaching 50% around r_{min}, as was already made clear by figure 2.8. The rest of the probability is distributed between 13 nm and 80 nm, so it seems reasonable to set at this distance a sort of border, and neglect the cases in which the CaV lies beyond it, since it is unlikely that the channel opening manages to activate the BK. We also notice that in about nine out of ten cases the BK opens when the calcium channel is located in the second shell, at distance $\leq 39\ nm$, meaning that, when only one CaV channel is considered, the discrete model will provide a good approximation of the dynamics.

On the other hand, if a second CaV channel is introduced, we need to analyse in detail all the possible configurations that can lead to the BK opening. In fact, when many CaVs are present, a plot of the cumulative probability of the open channels locations as the one in figure 2.9 would be deceiving, because every open CaV would be counted as a single event bringing to the BK activation, while everytime the BK opens it actually is the result of the combined action of all the CaVs which are active at that moment. Thus in table 2.1 we report the probabilities for every case, from which we can extract some interesting information. We immediately notice that the chances of observing a BK_{Ca}-CaV complex with both the calcium channels are very small: in comparison, the probability to have only one CaV bonded to the BK is one order of magnitude higher. Besides, these values indicate that about 70% of the time only one CaV

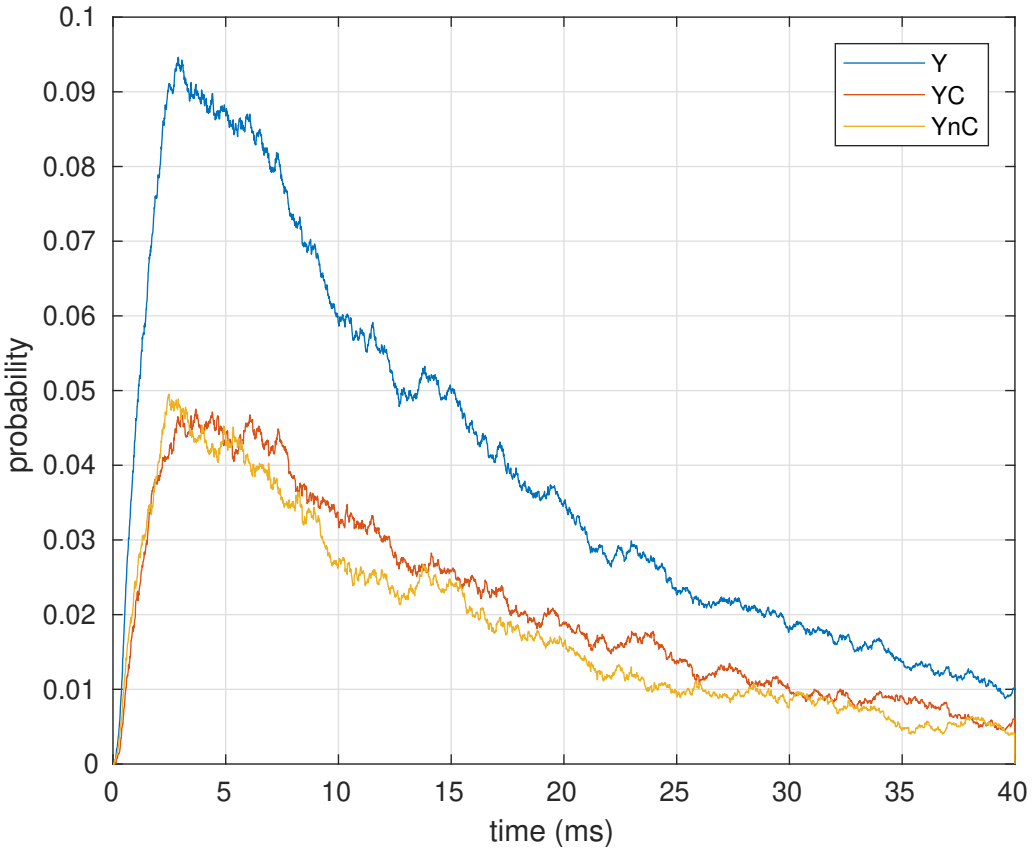

Figure 2.8: *BK open probability in time. Y indicates the total probability, YC is the complex contribution, YnC represents activation without the complex. The simulation was performed considering only one calcium channel and setting* $\tau = 0.1$ *ms as time step for the diffusion. It is interesting to note that the presence of the complex is not strictly necessary to observe the BK opening.*

is open, and this fact explains why the major contribution to the BK activation comes from the configurations in which one CaV is closed and the other one is bonded to the BK or is at distance ≤ 39 *nm*.

The study of the single calcium channel suggests that the activity of the CaVs which are at distance > 80 *nm* is not perceived by the BK, thus we want to quantify the actual contribution of the channels in the third shell also in the case where two channels are present. Therefore we exclude the open CaVs in the third shell from the calculation of the BK activation and deactivation rates, and we re-evaluate the probability for each combination of CaV states and distances to see how they are changed. The contributions that are actually being neglected are the elements in position $(5,1)$, $(1,5)$ and $(5,5)$ in table 2.1, that account for about 4% of the total BK open probability. Looking at table 2.2, we note that the probabilities of the other cases where one CaV is in the third shell, elements $2-4$ in row 5 and in column 5, appear to

CaV state/location	CaV 1 is closed	$r_1 \leq 13$	$13 < r_1 \leq 39$	$39 < r_1 \leq 80$	$r_1 > 80$
CaV 2 is closed	0.0000	0.1522	0.1137	0.0654	0.0191
$r_2 \leq 13$	0.1459	0.0123	0.0203	0.0296	0.0175
$13 < r_2 \leq 39$	0.1121	0.0205	0.0259	0.0301	0.0152
$39 < r_2 \leq 80$	0.0624	0.0312	0.0309	0.0217	0.0075
$r_2 > 80$	0.0216	0.0204	0.0162	0.0071	0.0011

Table 2.1: *Probability of every possible configuration that leads to the BK opening.*

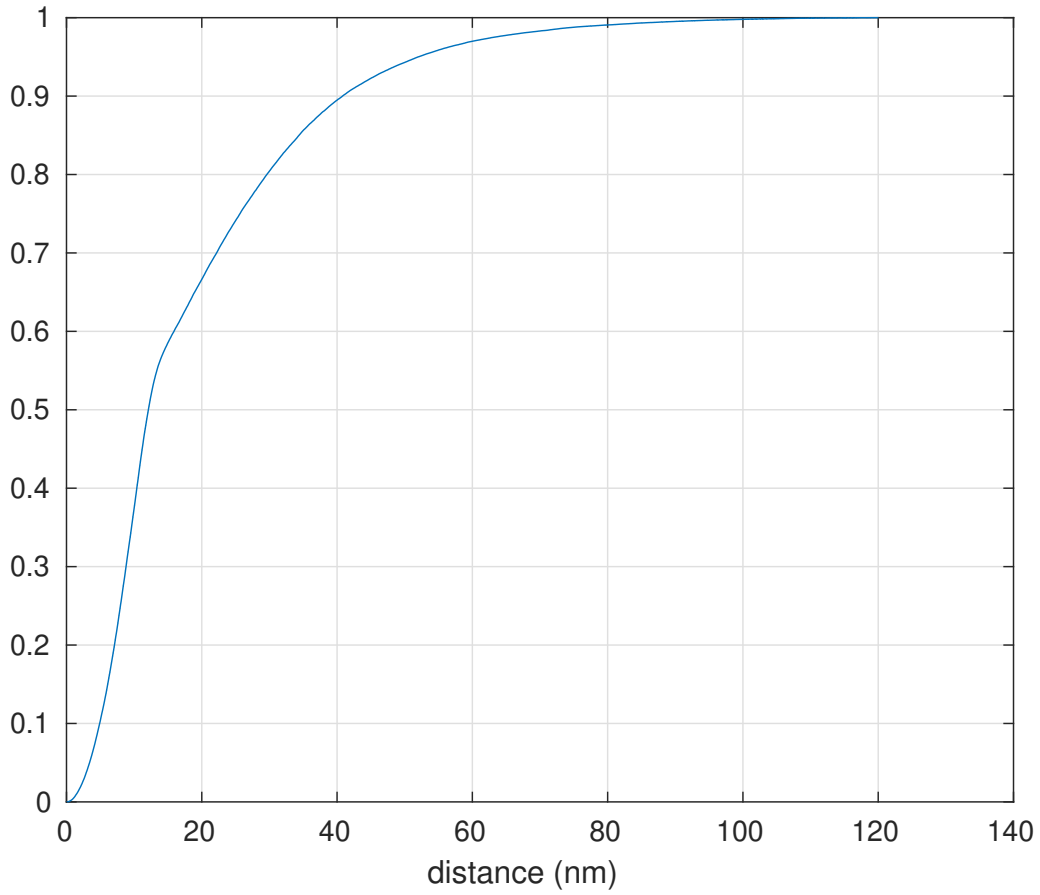

Figure 2.9: *Cumulative probability to find the CaV channel responsible for the BK opening within a certain distance from the BK. The initial steep slope represents the formation of the bond between the BK and the CaV.*

be summed up to the probabilities in cells $2-4$ in row 1 and in column 1, meaning that the presence of the open CaV at distance $> 80\ nm$ is not necessary to obtain the BK activation. We therefore identify a sort of dead zone between adiacent BKs, a region of the cell membrane where the action of the CaVs is basically neutralized by the distance, as the peak in the Ca^{2+} concentration that is produced when the calcium channels are open can not reach any of the surrounding BKs, and also when added to the Ca^{2+} flow provided by other open CaVs its effect is negligible.
The study of the shells population suggests that we could consider only a few distances, that represent the average behaviour of the channels, and construct a discrete model on a grid for which we would be able to write a Markov chain similar to the one presented in ([1]). In order to get a manageable set of equation we decide to consider only the first and the second shell, setting the border of the grid at distance $3r_{min} = 39\ nm$. If we perform the sum of the elements in row 4 and column 4 in table 2.2, we find that the choice not to include the third shell implies that we are practically neglecting 30% of the cases in which the BK is open.

In order to better understand how the CaV dynamics affects the BK open probability, we report in figure 2.11 the activation and deactivation rates for the BK in the case when the CaV is open. We notice that the opening rate $k_o^+(r)$ decreases rapidly as the CaV moves away from the BK.
As already highlighted, these rates depend on the Ca^{2+} concentration that is detected by the BK channel. When more than one CaV channel is present, and open, the linear buffer approximation ([9]) is used to combine the Ca^{2+} levels.

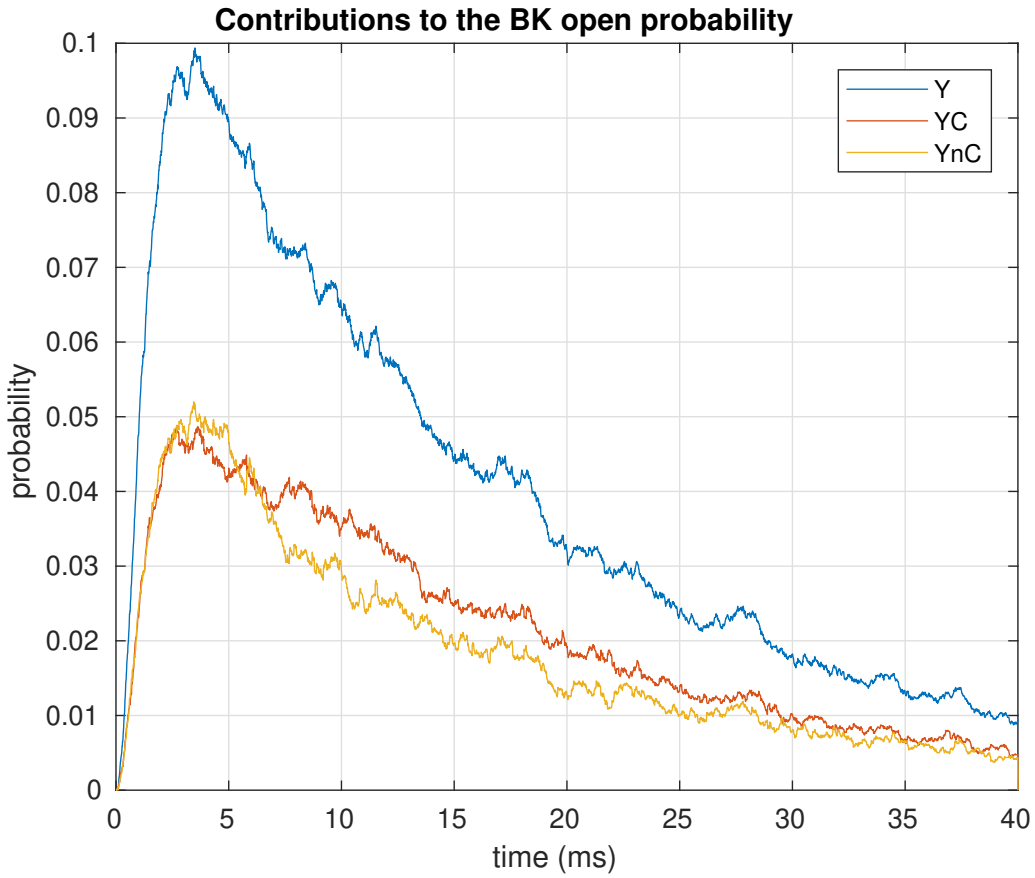

Figure 2.10: *Bk open probability calculated without taking into account the contribution of the CaV channels which are located at distance* > 80 *nm. Here two calcium channels are simulated.*

CaV state/location	CaV 1 is closed	$r_1 \leq 13$	$13 < r_1 \leq 39$	$39 < r_1 \leq 80$
CaV 2 is closed	0.0000	0.1730	0.1373	0.0727
$r_2 \leq 13$	0.1750	0.0114	0.0198	0.0352
$13 < r_2 \leq 39$	0.1363	0.0209	0.0277	0.0327
$39 < r_2 \leq 80$	0.0686	0.0346	0.0318	0.0233

Table 2.2: *Probability of every possible configuration that leads to the BK opening, without taking into account the calcium channels which are beyond* 80 *nm. Comparing these results to the ones in table 2.1 it is possible to get an idea of how the effects of the two calcium channels combine to make the BK channel activates.*

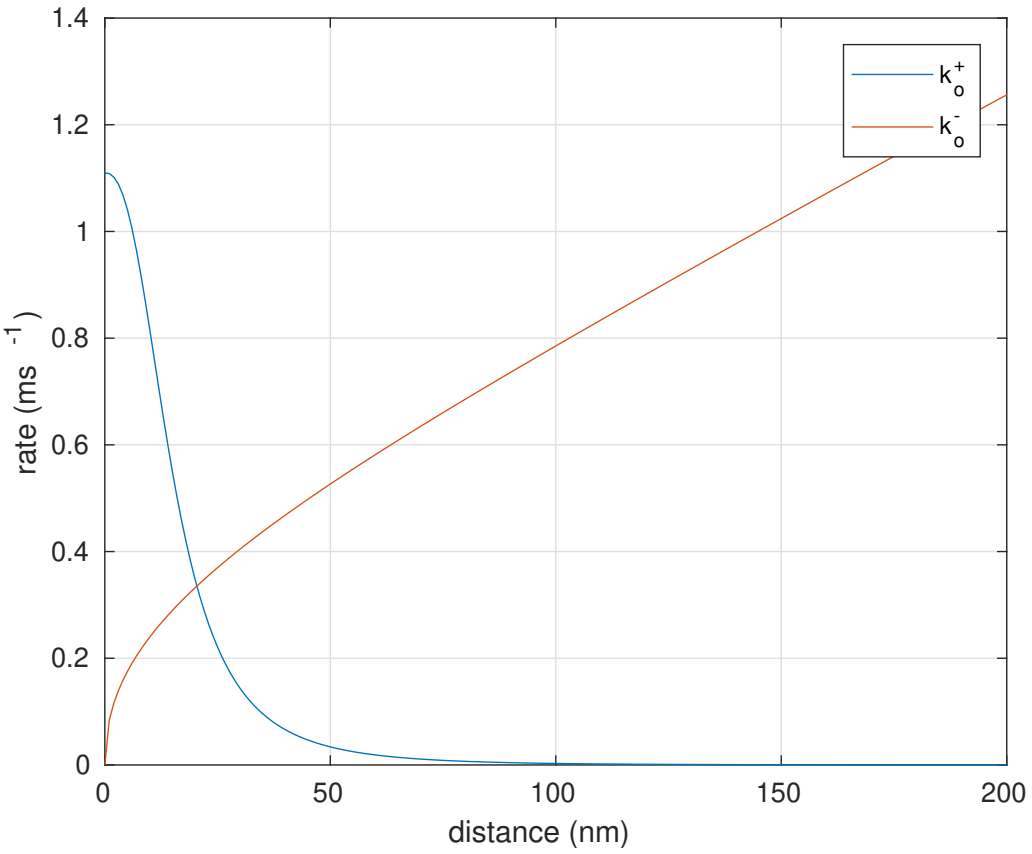

Figure 2.11: *BK opening and closing rates in presence of open CaV channels, evaluated as functions of the distance at which the source of* Ca^{2+} *ions is located.*

Chapter 3

Stochastic model of BK and CaV interaction with fixed distances

In chapter 1 we descibed the Markov chain model of the BK_{Ca}-Cav complex, devised to analyse the impact of the CaV dynamics on the BK activation when the two channels are bonded. In order to get a more realistic picture of ion channels interaction in the cell membrane we introduced in chapter 2 the CaV Brownian diffusion, and showed the characteristics of complex formation and its contribution to the BK open probability. The problem is that the mere Monte Carlo simulation does not provide us with much theoretical insight. Therefore our aim is to extend the model presented in Montefusco including the CaV diffusion around the BK, and in doing so we will obtain a new Markov chain and a new system of ODEs that constitute a more detailed description of ion channels activity.
Of course we can implement such a model only adding a few discrete states to the basic Markov chain, so we will realize the CaV diffusion as a two dimensional random walk on a series of points located at three different distances from the BK. In particular, we take a grid as the one in figure 3.1 and the distances considered are:

$$\begin{aligned} r_1 &= 13\ nm \\ r_2 &= r_1\sqrt{5} \simeq 29\ nm \\ r_3 &= 3r_1 = 39\ nm \end{aligned} \tag{3.1}$$

The unit length of the grid, meaning the distance between any two adiacent points, is $h = r_1\sqrt{2} \simeq 18.4\ nm$. In the previous chapter we have already estimated the limits of the approximation that we make neglecting the distances beyond r_3.
Assuming the number of CaVs that move around the BK is constant, being the membrane homogeneous, we impose periodic boundary conditions on the grid: if we label each one of the points as the element of a $4x4$ matrix, we have that, for example, going up from position $(1, 3)$ brings the channel in position $(3, 3)$, or going left from position $(2, 1)$ brings the CaV in position $(2, 3)$. Similarly, moving up from point $(1, 1)$ at distance r_3 the channel ends up in point $(3, 1)$ at distance r_2, while moving left it will reach point $(1, 3)$ again at distance r_2, and so on for all the other border locations.
Therefore we define a new three dimensional, 18-state, continuous-time Markov chain with three layers, one for each distance, and every layer is nothing but the basic 6-state Markov chain designed in ([1]), with the difference that now the BK opening and closing rates on every layer depend on the specific distance of the open CaV via the Ca^{2+} concentration that is perceived by the BK.
As we can see in figure 3.2, every state of this Markov chain is identified by three elements: the

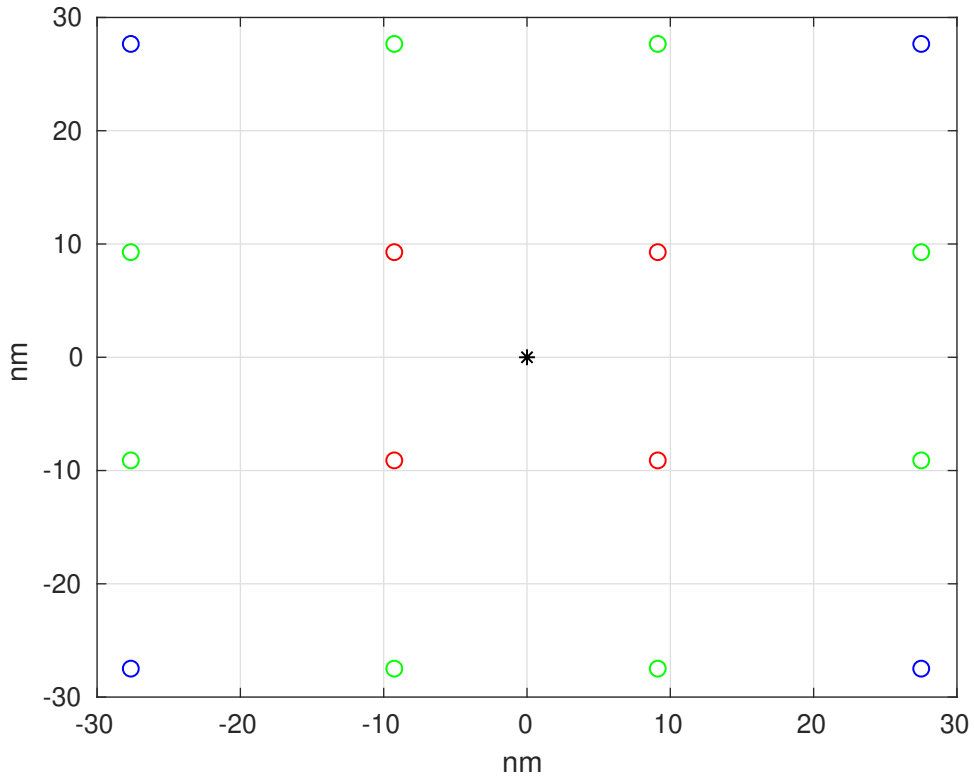

Figure 3.1: *Scheme of the grid where the CaV random walk will be simulated. The red points represent* $r_1 = 13$ *nm, the green points represent* $r_2 = 29$ *nm, the blue points represent* $r_3 = 39$ *nm. The unit length of the grid is* $h = 18.4$ *nm.*

CaV state, the BK state and the distance between the two channels.
The three layers are connected by the transition rates which control the CaV random walk on the grid. Since this is a continuous-time Markov chain, every movement of the calcium channel is described by a random variable $Exp\{\lambda\}$. We know that λ is the inverse of the expectation value of the exponential random variable which describes the single CaV movement. The random walk on the grid is the approximation of the free Brownian motion with diffusion coefficient $D_{free} = 0.035\ \mu m^2/s$ that the ion channel perform when it is not bonded to the BK. In this model, in fact, we can describe only a free diffusion with a single diffusion coefficient and we have to represent the formation of the BK_{Ca}-Cav complex multiplying the rate of breaking the bond between the two channels, that is j_{12}, by a factor that can take values in the interval $[0, 1]$. In this way, decreasing the value of the rate j_{12}, we express the fact that the CaV is less likely to leave its position at distance r_1 because it is bonded to the potassium channel.
Everytime the CaV moves it covers the distance h between two adiacent point on the grid. This movement correspond to a two-dimensional diffusion with mean squared displacement equal to h^2. Using the equation of Brownian motion, $MSD(t) = 4Dt$, we obtain that the time such a diffusion takes is $t = h^2/4D_{free}$, hence we define λ as the inverse of this time:

$$\lambda = \frac{4D_{free}}{h^2} = 0.41\ ms^{-1}. \tag{3.2}$$

Looking at figure 3.1 we note that from each point at distance r_1 it is possible to reach a point at distance r_2 in two ways, thus the random variable that express the channel going from r_1 to r_2 will be

$$min\{Exp\{\lambda\}, Exp\{\lambda\}\} = Exp\{2\lambda\}$$

and the correspondent transition rate will be $j_{12} = 2\lambda$. Following the same kind of reasoning,

we find all the rates for the random walk:

$$\begin{aligned} &r_1 \to r_2 : j_{12} = 2\lambda = 0.82\ ms^{-1} \\ &r_1 \to r_3 : j_{13} = 0 \\ &r_2 \to r_1 : j_{21} = 2\lambda = 0.82\ ms^{-1} \\ &r_2 \to r_3 : j_{23} = \lambda = 0.41\ ms^{-1} \\ &r_3 \to r_1 : j_{31} = 0 \\ &r_3 \to r_2 : j_{32} = 4\lambda = 1.64\ ms^{-1}. \end{aligned} \tag{3.3}$$

Since the CaV transitions between its states (closed, open and blocked) are independent of the channel diffusion on the membrane, the rates which control its dynamics must be left unchanged by the introduction of the random walk. To verify that the model is consistent with this assumption we write the total transition matrix for the calcium channel and we calculate the mean absorbing times in each one of its state. Imposing every one of these mean absorbing times to be equal to the inverse of the correspondent original rate, we find out that the transition rates for the dynamics remain the same.
Below the transition matrix for the calcium channel is reported (equation 3). The labels for both rows and columns are $\{C1, C2, C3, O1, O2, O3, B1, B2, B3\}$. The numbers 1, 2 and 3 refer to the distances r_1, r_2 and r_3.

$$Q_{CaV} = \begin{pmatrix} q_{11} & 2\lambda & 0 & \alpha & 0 & 0 & 0 & 0 & 0 \\ 2\lambda & q_{22} & \lambda & 0 & \alpha & 0 & 0 & 0 & 0 \\ 0 & 4\lambda & q_{33} & 0 & 0 & \alpha & 0 & 0 & 0 \\ \beta & 0 & 0 & q_{44} & 2\lambda & 0 & \delta & 0 & 0 \\ 0 & \beta & 0 & 2\lambda & q_{55} & \lambda & 0 & \delta & 0 \\ 0 & 0 & \beta & 0 & 4\lambda & q_{66} & 0 & 0 & \delta \\ 0 & 0 & 0 & \gamma & 0 & 0 & q_{77} & 2\lambda & 0 \\ 0 & 0 & 0 & 0 & \gamma & 0 & 2\lambda & q_{88} & \lambda \\ 0 & 0 & 0 & 0 & 0 & \gamma & 0 & 4\lambda & q_{99} \end{pmatrix} \tag{3.4}$$

The elements on the diagonal are given by $q_{ii} = -\sum_{j \neq i} q_{ij}$, so that the sum of the elements in every row is zero.
As regards the transition rates for the potassium channel, following the original model we set $k_c^+ \simeq 0$, because the background Ca_{2+} concentration is not sufficient to activate the BK. So, looking at the scheme in figure 3.2, we can say that all the transitions $CXi \to CYi$ and $BXi \to BYi$, for $i = 1, 2, 3$, are virtually impossible. Also the rate k_c^- depends on the background concentration of Ca_{2+}, so it does not change when introducing the three distances and it characterizes all the transitions $CYi \to CXi$ and $BYi \to BXi$ for $i = 1, 2, 3$.
The rates that are indeed affected by the calcium channel movement on the grid are k_o^+ and k_o^-, as they are calculated using the following espression for the Ca_{2+} concentration at the BK channel when the CaV is open:

$$Ca_o = \frac{g_{Ca}(V - V_{Ca}}{8\pi r D_{Ca} F} exp\left[\frac{-r}{\sqrt{\frac{D_{Ca}}{k_B^+ [B_{total}]}}}\right]. \tag{3.5}$$

This expression, that was already presented in chapter 1, shows a dependance on r, that is the distance between the open CaV and the BK. Therefore we will have $k_o^+(r_i)$ for the transition $OXi \to OYi$ and $k_o^-(r_i)$ for the transition $OYi \to OXi$, for $i = 1, 2, 3$. This means that the

transition matrix for the BK, that we can write in a general form as

$$Q_{BK} = \begin{pmatrix} -k^+ & k^+ \\ k^- & -k^- \end{pmatrix} \tag{3.6}$$

with labels $\{X, Y\}$ for both rows and columns, needs to be evaluated at every step in time, because the rates are calculated on the basis of the state and the position of the CaV channels at each instant.
At this point we have completely illustrated the model and we can proceed describing the Monte Carlo simulation of the channels activity.

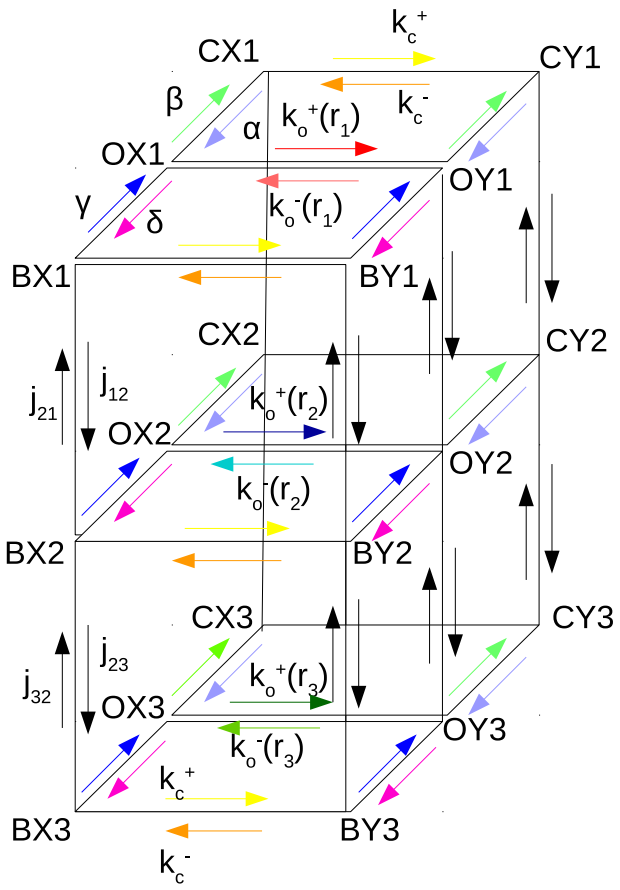

Figure 3.2: *Markov chain for the model with CaV random walk on the grid.*

3.1 Monte Carlo simulation

We consider only one calcium channel and, following ([1]), we set $\Delta t = 0.01\ ms$ as the time step. The initial conditions are set so that at time 0 both channels are closed and the CaV is located at distance $r - 3$.
In equations 3 and 3 we reported the matrices of the transition rates for the CaV and the BK channel. In order to perform the Monte Carlo simulation we need to construct the correspondent transition probabilities matrices:

$$P_{CaV} = \\ = \begin{pmatrix} P_{11} & 2\lambda\Delta t & 0 & \alpha\Delta t & 0 & 0 & 0 & 0 & 0 \\ 2\lambda\Delta t & P_{22} & \lambda\Delta t & 0 & \alpha\Delta t & 0 & 0 & 0 & 0 \\ 0 & 4\lambda\Delta t & P_{33} & 0 & 0 & \alpha\Delta t & 0 & 0 & 0 \\ \beta\Delta t & 0 & 0 & P_{44} & 2\lambda\Delta t & 0 & \delta\Delta t & 0 & 0 \\ 0 & \beta\Delta t & 0 & 2\lambda\Delta t & P_{55} & \lambda\Delta t & 0 & \delta\Delta t & 0 \\ 0 & 0 & \beta\Delta t & 0 & 4\lambda\Delta t & P_{66} & 0 & 0 & \delta\Delta t \\ 0 & 0 & 0 & \gamma\Delta t & 0 & 0 & P_{77} & 2\lambda\Delta t & 0 \\ 0 & 0 & 0 & 0 & \gamma\Delta t & 0 & 2\lambda\Delta t & P_{88} & \lambda\Delta t \\ 0 & 0 & 0 & 0 & 0 & \gamma\Delta t & 0 & 4\lambda\Delta t & P_{99} \end{pmatrix} \tag{3.7}$$

with labels $\{C1, C2, C3, O1, O2, O3, B1, B2, B3\}$ for both rows and columns. The expression of the elements on the diagonal is $P_{ii} = 1 - \sum_{j \neq i} P_{ij}\Delta t$.
Every element of the matrix represents the probability

$$P[S',\ t + \Delta t | S,\ t] \tag{3.8}$$

of a transition from state S to state S' over the time interval Δt, being S and S' any two states of the CaV.
In chapter 2 we carried out the simulation of the CaV diffusion and the dynamics between its state independently, as two separate processes, then the results were combined so that at every instant there were a position and a state associated to the channel. On the other hand, in the Markov chain we are treating now the CaV is already described by a pair of the form (SD), where S indicates the state and D stand for the distance respect to the BK and the transitions are realized between these composed states. This means that, at every step in time, the new condition of the CaV is the result of the competition between the exponential random variables that represent all the possible transitions from the current composed state. In other words, over one Δt the calcium channel can change its state (C, O, B) or its distance from the BK, or it can stay the same.
Similarly, for the BK channel we write:

$$P_{BK} = \begin{pmatrix} 1 - k^+\Delta t & k^+\Delta t \\ k^-\Delta t & 1 - k^-\Delta t \end{pmatrix} \tag{3.9}$$

with labels $\{X, Y\}$ for both rows and columns. While the elements of the probability matrix for the CaV are constant, the BK probability matrix needs to be updated at each time step, because the rates have to be re-evaluated on the basis of the CaV state and location at that moment.
The procedure used to perform the simulation is the following. Given the current state of the CaV, we take the matrix elements in the row corresponding to that state and use them to divide the interval $[0, 1]$ in a series of subintervals. For example, if the CaV is in $C3$, we can define the subintervals $[0, 1 - (\alpha + 4\lambda)\Delta t[$, $[1 - (\alpha + 4\lambda)\Delta t, 1 - \alpha\Delta t[$ and $[1 - \alpha\Delta t, 1]$. Then we

generate a random number ξ from a uniform distribution on the interval $[0, 1]$: the transition will be determined by the subinterval in which ξ falls. In the case of $C3$, if ξ is in the first subinterval the CaV remains in the same state, if $1 - (\alpha + 4\lambda)\Delta t \leq \xi \leq 1 - \alpha\Delta t$ then the channel moves on the grid and the updated state is $C2$, otherwise, if $\xi \geq 1 - \alpha\Delta t$, a transition to the open state $O3$ occurs. The CaV state that is reached in this way is immediately used to calculate the proper transition rates for the BK. Next, another random number η uniformly distributed on $[0, 1]$ is chosen and the operation just described has to be repeated, but it is a bit simpler because for the BK we always have only two subintervals: if $\eta \leq P_{BK}(i, i)$ the BK state is left unchanged, otherwise a transition to the other state is observed.
The results of the simulation will be shown below, in comparison with the one that will be obtained in the next section.

3.2 ODE model

Following Montefusco, we aim to define also in this case a deterministic model of the BK activity at cellular level, in order to obtain a whole-cell BK current. This current, as already explained in chapter 1, is given by the expression:

$$I_{BK} = g_{BK} p_Y (V - V_K) \tag{3.10}$$

where g_{BK} is the maximal whole-cell BK conductance and V_K is the K^+ reversal potential. Thus we need to understand how the BK open probability p_Y behaves over time, and to do that we have to study the time evolution of the probability distribution of our 18-state Markov chain. The equations for every state of the system are reported below (eq. 3.2). To simplify the notation from now on we indicate the probability of a state with the name of the state, for example $CX1$ stands for P_{CX1}.
Since the probabilities must sum to 1, taking a system of 17 of the differential equations in 3.2 is sufficient to know the evolution in time of the probabilities for every state of the system. So first we solve this ODE system, that certainly represents a reduction respect to the Monte Carlo simulations. However it is also clear that the introduction of the CaV diffusion on the grid increases the complexity of the problem in comparison to the system of 5 ODEs treated in ([1]). Therefore we try to simplify this system, in order to see if it is possible to get to a smaller set of equations. In particular, we would like to obtain the time evolution for the activation variable m_{BK}, that express the fraction of open BK channels in presence of non-inactivated CaVs. Below the details of the calculations are illustrated.
We know that, as it can be seen in figure 3.3, inactivation and reactivation of CaV channels are slower processes than opening and closing and these two time scales can be separated. So we consider two submodels, one for non-inactivated CaVs, with 12 states, and one for the CaVs that are blocked, with 6 states. So we proceed working on the reduced system of 12 equations for non-inactivated CaVs reported below in equation 3.2.

$$
\begin{aligned}
\frac{dCX1}{dt} &= j_{21}CX2 + \beta OX1 + k_c^- CY1 - (j_{12} + \alpha)CX1 \\
\frac{dCX2}{dt} &= j_{12}CX1 + j_{32}CX3 + \beta OX2 + k_c^- CY2 - (j_{21} + j_{23} + \alpha)CX2 \\
\frac{dCX3}{dt} &= j_{23}CX2 + \beta OX3 + k_c^- CY3 - (j_{32} + \alpha)CX3 \\
\frac{dOX1}{dt} &= j_{21}OX2 + \alpha CX1 + \gamma BX1 + k_o^-(r_1)OY1 - (j_{12} + \beta + \delta + k_o^+(r_1))OX1 \\
\frac{dOX2}{dt} &= j_{12}OX1 + j_{32}OX3 + \alpha CX2 + \gamma BX2 + k_o^-(r_2)OY2 - (j_{21} + j_{23} + \beta + \delta + k_o^+(r_2))OX2 \\
\frac{dOX3}{dt} &= j_{23}OX2 + \alpha CX3 + \gamma BX3 + k_o^-(r_3)OY3 - (j_{32} + \beta + \delta + k_o^+(r_3))OX3 \\
\frac{dBX1}{dt} &= j_{21}BX2 + \delta OX1 + k_c^- BY1 - (j_{12} + \gamma)BX1 \\
\frac{dBX2}{dt} &= j_{12}BX1 + j_{32}BX3 + \delta OX2 + k_c^- BY2 - (j_{21} + j_{23} + \gamma)BX2 \\
\frac{dBX3}{dt} &= j_{23}BX2 + \delta OX3 + k_c^- BY3 - (j_{32} + \gamma)BX3 \\
\frac{dCY1}{dt} &= j_{21}CY2 + \beta OY1 - (j_{12} + \alpha + k_c^-)CY1 \\
\frac{dCY2}{dt} &= j_{12}CY1 + j_{32}CY3 + \beta OY2 - (j_{21} + j_{23} + \alpha + k_c^-)CY2 \\
\frac{dCY3}{dt} &= j_{23}CY2 + \beta OY3 - (j_{32} + \alpha + k_c^-)CY3 \\
\frac{dOY1}{dt} &= j_{21}OY2 + \alpha CY1 + \gamma BY1 + k_o^+(r_1)OX1 - (j_{12} + \beta + \delta + k_o^-(r_1))OY1 \\
\frac{dOY2}{dt} &= j_{12}OY1 + j_{32}OY3 + \alpha CY2 + \gamma BY2 + k_o^+(r_2)OX2 - (j_{21} + j_{23} + \beta + \delta + k_o^-(r_2))OY2 \\
\frac{dOY3}{dt} &= j_{23}OY2 + \alpha CY3 + \gamma BY3 + k_o^+(r_3)OX3 - (j_{32} + \beta + \delta + k_o^-(r_3))OY3 \\
\frac{dBY1}{dt} &= j_{21}BY2 + \delta OY1 - (j_{12} + \gamma + k_c^-)BY1 \\
\frac{dBY2}{dt} &= j_{12}BY1 + j_{32}BY3 + \delta OY2 - (j_{21} + j_{23} + \gamma + k_c^-)BY2 \\
\frac{dBY3}{dt} &= j_{23}BY2 + \delta OY3 - (j_{32} + \gamma + k_c^-)BY3
\end{aligned}
\tag{3.11}
$$

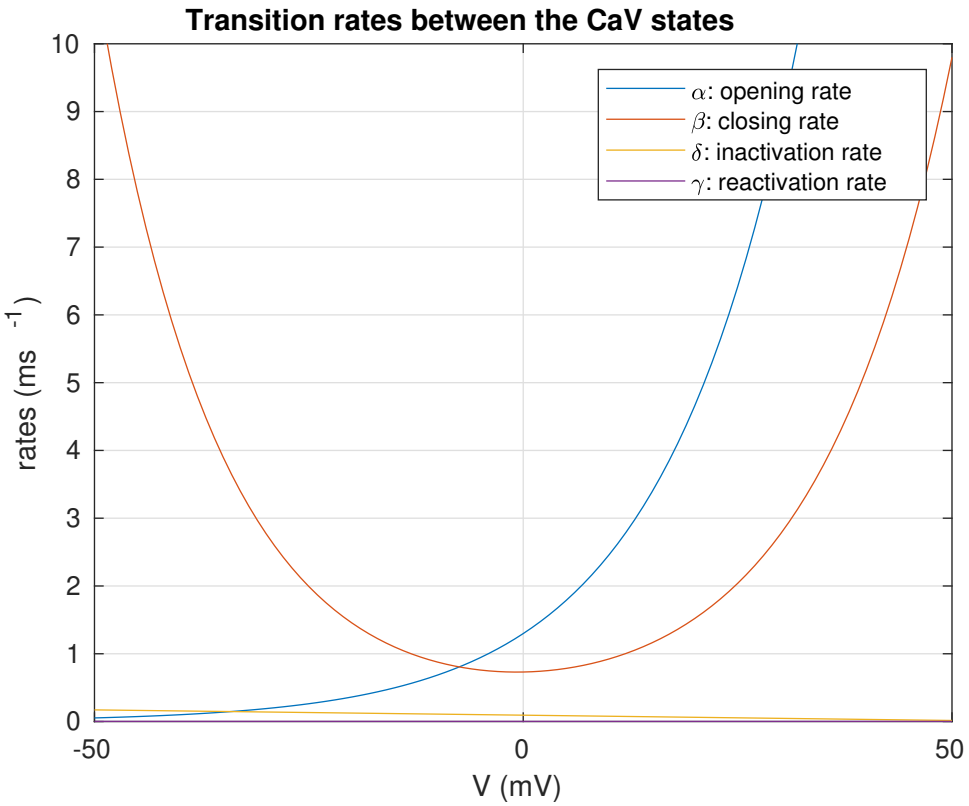

Figure 3.3: *Rates that regulate the dynamics of the CaV channel, as function of the membrane voltage. At 0 mV, the voltage we use for the calculations, the processes of inactivation and reactivation are slower in comparison to the channel opening and closing.*

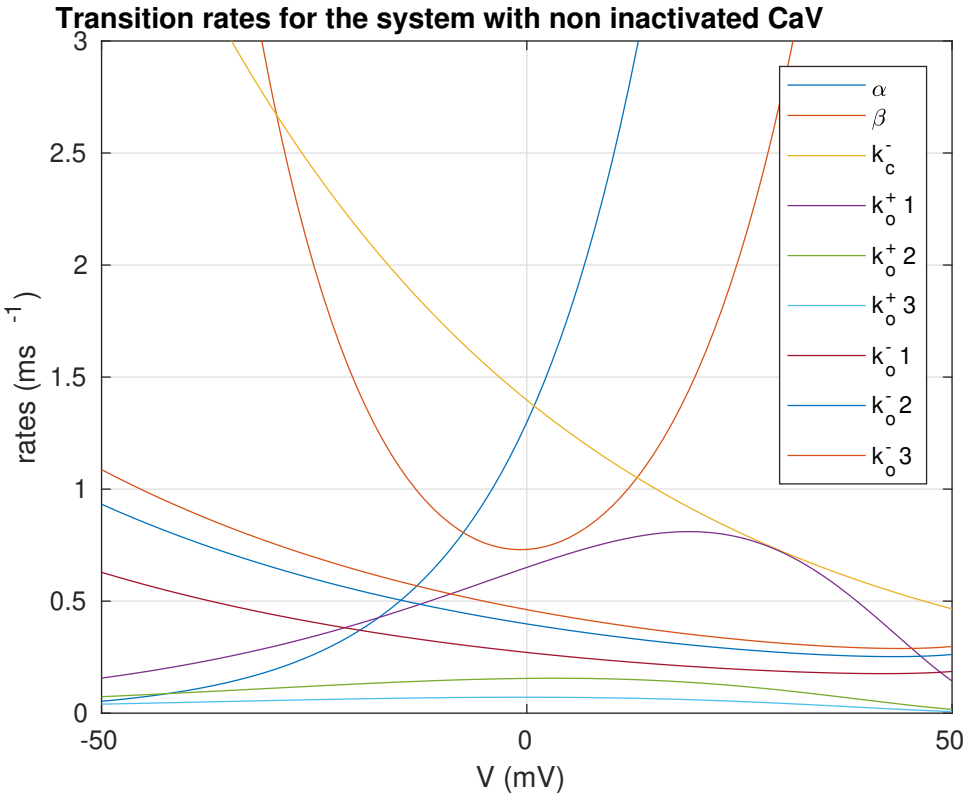

Figure 3.4: *Overview of all the rates at play in presence of non inactivated CaV channels, as function of the membrane voltage.*

$$
\begin{aligned}
\frac{dCX1}{dt} &= j_{21}CX2 + \beta OX1 + k_c^- CY1 - (j_{12} + \alpha)CX1 \\
\frac{dCX2}{dt} &= j_{12}CX1 + j_{32}CX3 + \beta OX2 + k_c^- CY2 - (j_{21} + j_{23} + \alpha)CX2 \\
\frac{dCX3}{dt} &= j_{23}CX2 + \beta OX3 + k_c^- CY3 - (j_{32} + \alpha)CX3 \\
\frac{dOX1}{dt} &= j_{21}OX2 + \alpha CX1 + k_o^-(r_1)OY1 - (j_{12} + \beta + k_o^+(r_1))OX1 \\
\frac{dOX2}{dt} &= j_{12}OX1 + j_{32}OX3 + \alpha CX2 + k_o^-(r_2)OY2 - (j_{21} + j_{23} + \beta + k_o^+(r_2))OX2 \\
\frac{dOX3}{dt} &= j_{23}OX2 + \alpha CX3 + k_o^-(r_3)OY3 - (j_{32} + \beta + k_o^+(r_3))OX3 \\
\frac{dCY1}{dt} &= j_{21}CY2 + \beta OY1 - (j_{12} + \alpha + k_c^-)CY1 \\
\frac{dCY2}{dt} &= j_{12}CY1 + j_{32}CY3 + \beta OY2 - (j_{21} + j_{23} + \alpha + k_c^-)CY2 \\
\frac{dCY3}{dt} &= j_{23}CY2 + \beta OY3 - (j_{32} + \alpha + k_c^-)CY3 \\
\frac{dOY1}{dt} &= j_{21}OY2 + \alpha CY1 + k_o^+(r_1)OX1 - (j_{12} + \beta + k_o^-(r_1))OY1 \\
\frac{dOY2}{dt} &= j_{12}OY1 + j_{32}OY3 + \alpha CY2 + k_o^+(r_2)OX2 - (j_{21} + j_{23} + \beta + k_o^-(r_2))OY2 \\
\frac{dOY3}{dt} &= j_{23}OY2 + \alpha CY3 + k_o^+(r_3)OX3 - (j_{32} + \beta + k_o^-(r_3))OY3
\end{aligned}
\tag{3.12}
$$

The activation variable for the BK is then $m_{BK} = CY + OY$, while the one for the CaV is $m_{CaV} = OX + OY$. In the case we are discussing, OY represents the sum of the probabilities that the BK is open, given that the open CaV channel is located at distance r_1, r_2 or r_3. The same is valid for CY and OX. If we define new activation variables that correspond to each one of the distances on the grid, we can write $m_{BK}i = CYi + OYi$ and $m_{CaV}i = OXi + OYi$ for $i = 1, 2, 3$, so that

$$
\begin{aligned}
m_{BK} &= m_{BK}1 \cdot P1 + m_{BK}2 \cdot P2 + m_{BK}3 \cdot P3 \\
m_{CaV} &= m_{CaV}1 \cdot P1 + m_{CaV}2 \cdot P2 + m_{CaV}3 \cdot P3.
\end{aligned}
\tag{3.13}
$$

where the weights Pi are the probabilities of the CaV channel being at distance r_1, r_2 or r_3, and, as we will see below, can be calculated using a set of differential equations that are independent of the rest of the dynamics. Now we substitute everywhere $OXi = m_{CaV}i - OYi$ and then $OYi = m_{BK}i - CYi$ and we are left with a system of 12 ODEs for the quantities: CXi, CYi, $m_{CaV}i$ and $m_{BK}i$ for $i = 1, 2, 3$.

In figure 3.4 it is possible to notice that at $V = 0\ mV$, the voltage we consider for the calculations, the fastes transitions are the ones described by α, β and k_c^-, meaning the opening and closing dynamics of the CaV and the deactivation of the BK when the CaV is closed and there is only the background concentration of Ca^{2+} ions. This fact leads us to assume quasi-steady states for the probabilities CYi, thus we set

$$
\frac{dCYi}{dt} \simeq 0 \ \forall i
$$

It will be verified later that the time scale of the CYi is actually fast compared to the time scale of the $mBKi$, thus we can consider the CYi constant during the evolution of the $m_{BK}i$. From the conditions of quasi-steady state for the CYi we derive these three expressions:

$$
\begin{aligned}
CY1 &= \frac{j_{21}CY2 + \beta m_{BK}1}{j_{12} + \alpha + \beta + k_c^-} \\
CY2 &= \frac{j_{12}CY1 + j_{32}CY3 + \beta m_{BK}2}{j_{21} + j_{23} + \alpha + \beta + k_c^-} \\
CY3 &= \frac{j_{23}CY2 + \beta m_{BK}3}{j_{32} + \alpha + \beta + k_c^-}.
\end{aligned} \tag{3.14}
$$

To simplify the notation we will call:

$$
\begin{aligned}
A &= \alpha + \beta + k_c^- \\
A1 &= j_{12} + A \\
A2 &= j_{21} + j_{23} + A \\
A3 &= j_{32} + A.
\end{aligned} \tag{3.15}
$$

From these quantities we get the time constants for the CYi: in fact $\tau_{CY1} = 1/A1$, $\tau_{CY2} = 1/A2$ and $\tau_{CY3} = 1/A3$.
We proceed manipulating these equations in order to obtain expressions for the CYi that are function only of the transitions rates and of the $m_{BK}i$. Of course such expressions will not be easy to interpret theoretically, mainly because the dependance on the transition rates is quite complicated and it is not straigthforward to recognize the different contributes. The final result is:

$$
\begin{aligned}
CY1 &= \frac{\beta}{B}\left[m_{BK}1(A2A3 - j_{23}j_{32}) + m_{BK}2j_{21}A3 + m_{BK}3j_{32}j_{21}\right] \\
CY2 &= \frac{\beta}{B}\left[m_{BK}1j_{12}A3 + m_{BK}2A1A3 + m_{BK}3j_{32}A1\right] \\
CY3 &= \frac{\beta}{B}\left[m_{BK}1j_{12}j_{23} + m_{BK}2j_{23}A1 + m_{BK}3(A1A2 - j_{12}j_{21})\right]
\end{aligned} \tag{3.16}
$$

where $B = A1A2A3 - j_{21}j_{12}A3 - j_{23}j_{32}A1$.
Next we insert the expressions found for the CYi in the differential equations fo the $m_{BK}i$ and computing the calculations we obtain:

$$
\frac{dm_{BK}1}{dt} = \frac{m_{BK}1_\infty - m_{BK}1}{\tau_{m1}} \tag{3.17}
$$

$$
\frac{dm_{BK}2}{dt} = \frac{m_{BK}2_\infty - m_{BK}2}{\tau_{m2}} \tag{3.18}
$$

$$
\frac{dm_{BK}3}{dt} = \frac{m_{BK}3_\infty - m_{BK}3}{\tau_{m3}}. \tag{3.19}
$$

The $m_{BK}i_\infty$ are the steady states and they are given by:

$$
\begin{aligned}
m_{BK}1_\infty =& (k_o^+1 \cdot m_{CaV}1 + m_{BK}2j_{21}\left[1 + \frac{\beta}{B}A3(k_o^-1 + k_o^+1 - k_c^-)\right] + \\
&+ m_{BK}3j_{21}j_{32}\frac{\beta}{B}(k_o^-1 + k_o^+1 - k_c^-) \cdot \tau_{m1}
\end{aligned} \tag{3.20}
$$

$$
\begin{aligned}
m_{BK}2_\infty =&(k_o^+2 \cdot m_{CaV}2 + m_{BK}1 j_{12} \left[1 + \frac{\beta}{B} A3(k_o^-2 + k_o^+2 - k_c^-)\right] + \\
&+ m_{BK}3 j_{32} \left[1 + \frac{\beta}{B} A1(k_o^-2 + k_o^+2 - k_c^-)\right]) \cdot \tau_{m2}
\end{aligned} \tag{3.21}
$$

$$
\begin{aligned}
m_{BK}3_\infty =&(k_o^+3 \cdot m_{CaV}3 + m_{BK}2 j_{23} \left[1 + \frac{\beta}{B} A1(k_o^-3 + k_o^+3 - k_c^-)\right] + \\
&+ m_{BK}1 j_{12} j_{23} \frac{\beta}{B}(k_o^-3 + k_o^+3 - k_c^-)) \cdot \tau_{m3}.
\end{aligned} \tag{3.22}
$$

The τ_{mi} are the time constants and they depend on the transition rates of the system:

$$
\begin{aligned}
\tau_{m1} =&(j_{12} + \beta + k_o^+1 + k_o^-1 + \frac{\beta}{B} j_{12} j_{21} A3 - \\
&- \frac{b}{B}(A2A3 - j_{23} j_{32})(j_{12} + \alpha + \beta + k_o^+1 + k_o^-1))^{-1}
\end{aligned} \tag{3.23}
$$

$$
\begin{aligned}
\tau_{m2} =&(j_{21} + j_{23} + \beta + k_o^+2 + k_o^-2 + \frac{\beta}{B} j_{12} j_{21} A3 + \frac{\beta}{B} j_{23} j_{32} A1 - \\
&- \frac{\beta}{B} A1A3(j_{21} + j_{23} + \alpha + \beta + k_o^+2 + k_o^-2))^{-1}
\end{aligned} \tag{3.24}
$$

$$
\begin{aligned}
\tau_{m3} =&(j_{32} + \beta + k_o^+3 + k_o^-3 + \frac{\beta}{B} j_{23} j_{32} A1 - \\
&- \frac{\beta}{B}(A1A2 - j_{21} j_{12})(j_{32} + \alpha + \beta + k_o^+3 + k_o^-3))^{-1}.
\end{aligned} \tag{3.25}
$$

So, to summurize what we did up to this point, starting from a system with 12 ODEs and using appropriate time scale analysis and mathematical manipulation, we were able to eliminate the three ODEs for the probabilities CYi and we found explicit expressions for the three ODEs that describe the evolution of the BK activation variables, the $m_{BK}i$. We note that, because of the CaV random walk on the grid, equations 3.2-3.2 are not independent from each other. Besides, these equations are defined only in terms of the activation variables of both the BK and the CaV.
Through a similar kind of calculations we are able to write analogue differential equations for the CaV activation variables $m_{CaV}i$. But before doing that it is useful to consider the other set of three ODEs that we have, the one that guides the evolution of the probabilities CXi. In the original model in Montefusco the equation for CX was not necessary thanks to the conservation of the total probability, but this method can not be applied now. A possible solution is to introduce new variables Pi, that represent the probabilities of the non-inactivated CaV being at distance r_i. The form of these variables is then $Pi = CXi + CYi + m_{CaV}i$ and for them we can define a system that is independent from the equations for the other probabilities at play, and for this reason it can be immediately solved. In fact we have:

$$
\begin{aligned}
&\frac{dP1}{dt} = j_{21} P2 - j_{12} P1 \\
&\frac{dP2}{dt} = (j_{12} - j_{32}) P1 - (j_{21} + j_{23} + j_{32}) P2 + j_{32} \\
&P3 = 1 - P1 - P2.
\end{aligned} \tag{3.26}
$$

So it appear convenient to insert the expressions $Pi - CYi - m_{CaV}i$ in place of the CXi that occurr in the equations for the CaV activation variables. The advantage of eliminating the probabilities CXi from the ODE system is that we can now substitute the ODEs for the CXi with the two equations for the Pi. This way we are left with a system of 8 ODEs: three for the

$m_{BK}i$, three for the $m_{CaV}i$ and two for the Pi, which can be solved separately from the other six.
Through some mathematical manipulation we finally arrive at the equations for the CaV activation variables:

$$\begin{aligned}
\frac{dm_{CaV}1}{dt} &= j_{21}m_{CaV}2 + \alpha P1 - m_{CaV}1(\alpha + \beta + j_{12}) \\
\frac{dm_{CaV}2}{dt} &= j_{12}m_{CaV}1 + j_{32}m_{CaV}3 + \alpha P2 - m_{CaV}2(\alpha + \beta + j_{21} + j_{23}) \\
\frac{dm_{CaV}3}{dt} &= j_{23}m_{CaV}2 + \alpha P3 - m_{CaV}3(\alpha + \beta + j_{32})
\end{aligned} \tag{3.27}$$

Also in this case we can write the time constants and the steady states:

$$\begin{aligned}
&\tau_{mCaV}1 = (\alpha + \beta + j_{12})^{-1} \\
&\tau_{mCaV}2 = (\alpha + \beta + j_{21} + j_{23})^{-1} \\
&\tau_{mCaV}3 = (\alpha + \beta + j_{32})^{-1} \\
&m_{CaV}1_{\infty} = (j_{21}m_{CaV}2 + \alpha P1) \cdot \tau_{mCaV}1 \\
&m_{CaV}2_{\infty} = (j_{12}m_{CaV}1 + j_{32}m_{CaV}3 + \alpha P2) \cdot \tau_{mCaV}2 \\
&m_{CaV}3_{\infty} = (j_{23}m_{CaV}2 + \alpha P3) \cdot \tau_{mCaV}3
\end{aligned} \tag{3.28}$$

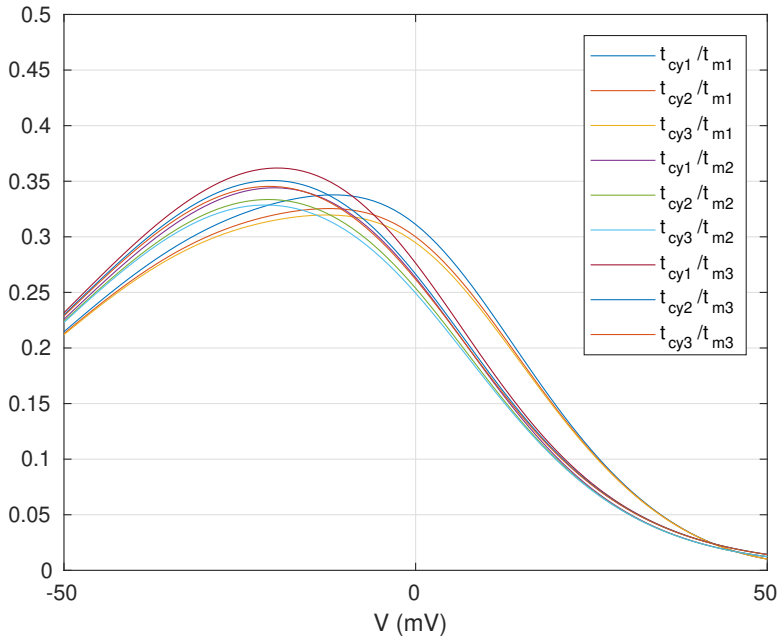

Figure 3.5: *Relationship between the time constants of the CYi and the $m_{BK}i$. The value of these ratios at $V = 0\ mV$ is essentially the same found for the correspondent quantity in [1], hence also in our case it is possible to consider steady states for the CYi as the $m_{BK}i$ evolve on a slower time scale.*

To conclude this description of the deterministic model, we report in figure 3.5 the plot that confirms the fact that the $m_{BK}i$ and the CYi evolve on different time scales, namely the dynamics of the CYi is faster than the dynamics of the BK activation variables, as we can see from the relationship between the correspondent time constant. This fact enables us to take the CYi as constants when studying the evolution of the $m_{BK}i$.
Now we can proceed solving the system. The results will be presented in the next section in comparison with the ones obtained from the Monte Carlo simulation.

3.3 Discussion of the results

The first aspect we want to analyze is the CaV diffusion on the grid. Given the transitions rates in equation 3, we follow the time evolution of the probability of the CaV being at a certain distance from the BK. Two methods are used: the ODE system for the Pi, reported in equation 3.2, and the Monte Carlo simulation of the Markov chain that represents the channel activity, based on the matrix of the transition probabilities 3.1.
As we have already said, in this model the formation of the BK_{Ca}-CaV complex is described through the multiplication of the rate j_{12} by a factor that weakens it, because the probability of leaving the points at distance r_1 is decreased by the presence of the bond between the two channels. We call this factor *bond* and it can take values in the interval $[0, 1]$. Figure 3.6 shows the evolution of the probabilities Pi in the case of $bond = 1$, that means considering the CaV movement without the transient anchorage due to the bond formation, in other words in the absence of the BK. Starting from a point at distance r_3, in a few milliseconds the calcium channel reaches a stable situation in which the probability of being at each one of the three distances remains constant. So, when the CaV is driven only by the rules that are the product of the grid configuration, after an initial transient it spends 10% of its time in location at distance r_3, while in the rest of the time it can be found indifferently at distance r_1 or r_2. Both the methods used bring to the same result.

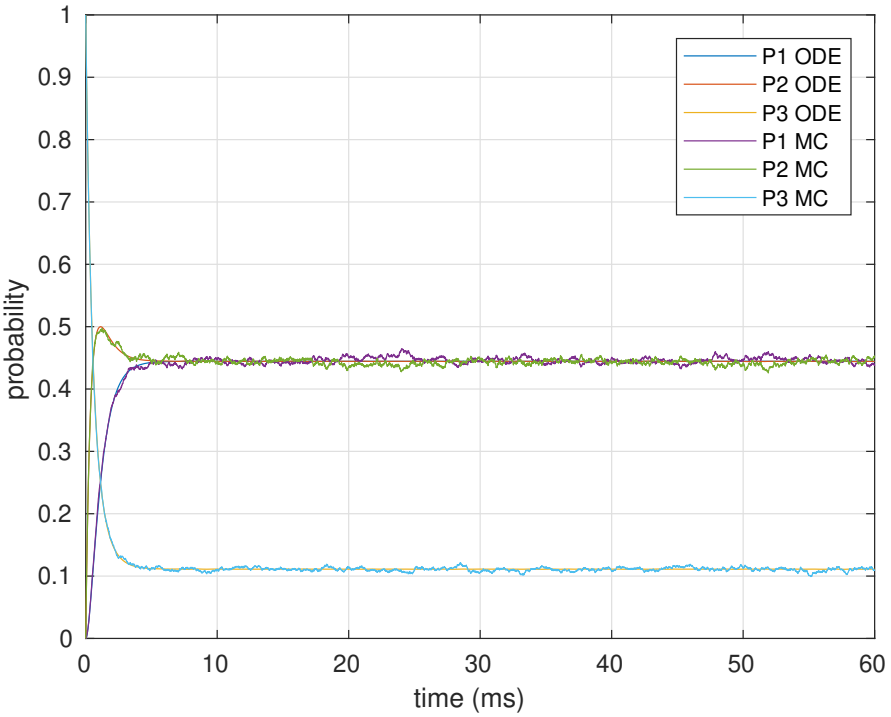

Figure 3.6: *Time evolution for the probabilities of the CaV channel being at distance r_1, r_2 or r_3. The variable bond is set equal to 1, meaning this is the evolution of the CaV movement on the grid without considering the transient anchorage to the BK.*

Now the problem is to set the proper value for the variable *bond*, so that the random walk on the grid can actually approximate the CaV diffusion in presence of the BK. To do that we refer to the Monte Carlo simulation of the CaV Brownian motion that was presented in chapter 2. We perform the simulation setting $r_3 = 39\ nm$ as outer border and we obtain figure 3.7. This plot shows that under these conditions the complex contribution to the BK open probability is about 60% of the total. So we choose the value for *bond* in such a way to be able to reproduce these proportions with the grid model. We find that setting $bond = 0.5$ produces figure 3.8 and we will use this value in the rest of the work.

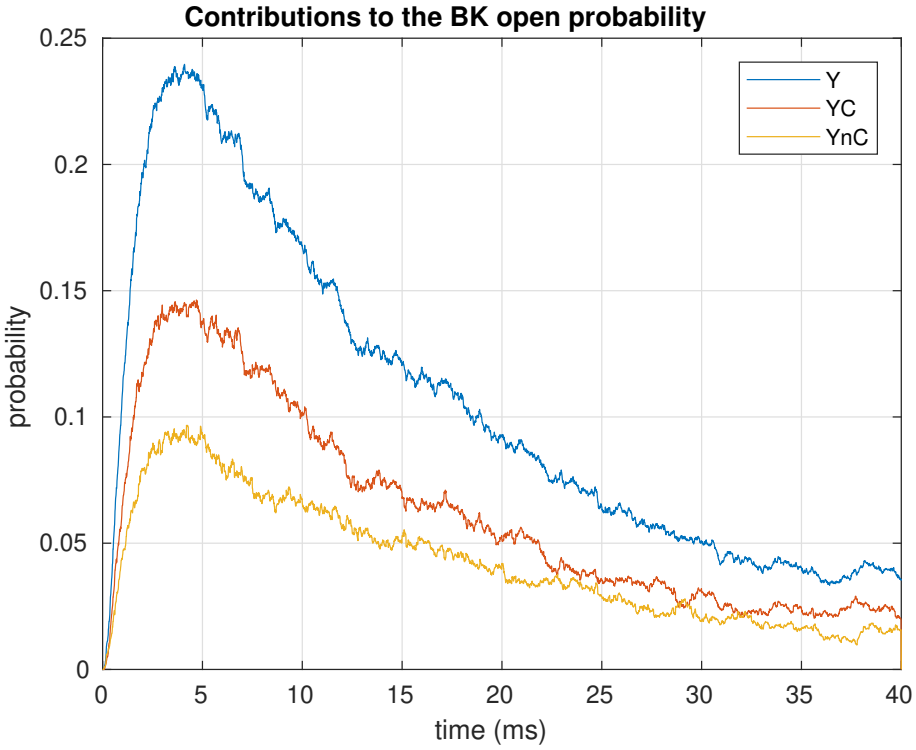

Figure 3.7: *BK open probability obtained using the Monte Carlo simulation presented in chapter 2, this time taking $r = 39$ nm as outer border for the BK area, so that we are reproducing the same spatial conditions of the grid. Since the area over which the CaV channel can move is now smaller, the probability that it bonds with the BK is higher and as a consequence the contribution of the complex becomes more important.*

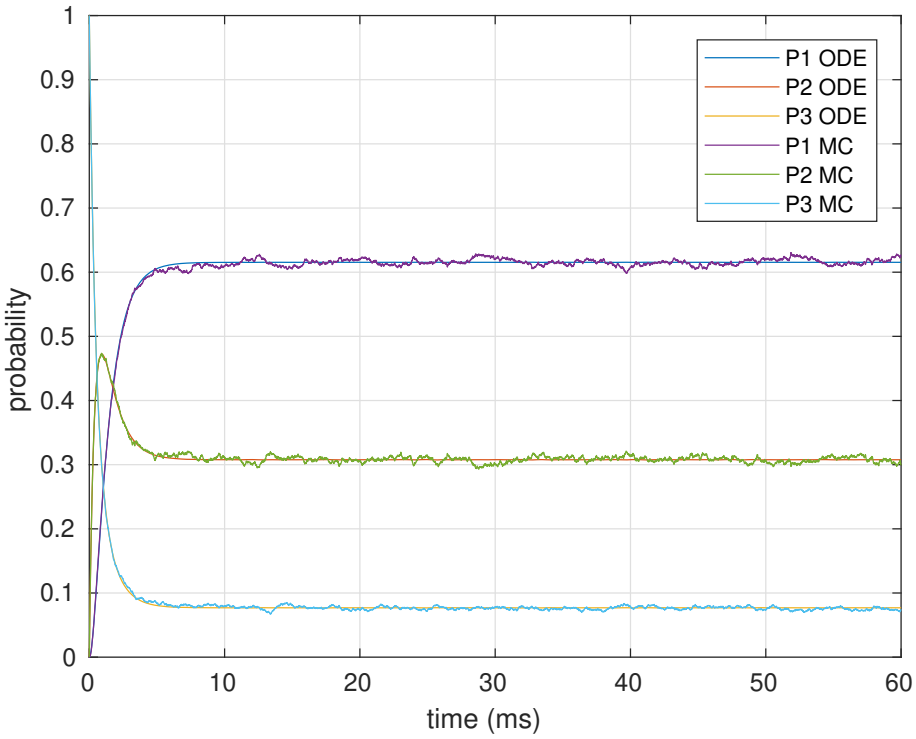

Figure 3.8: *Time evolution for the probabilities of the CaV channel being at distance r_1, r_2 or r_3, having set bond $= 0.5$ to represent the strength of the bond between the CaV channel and the BK channel.*

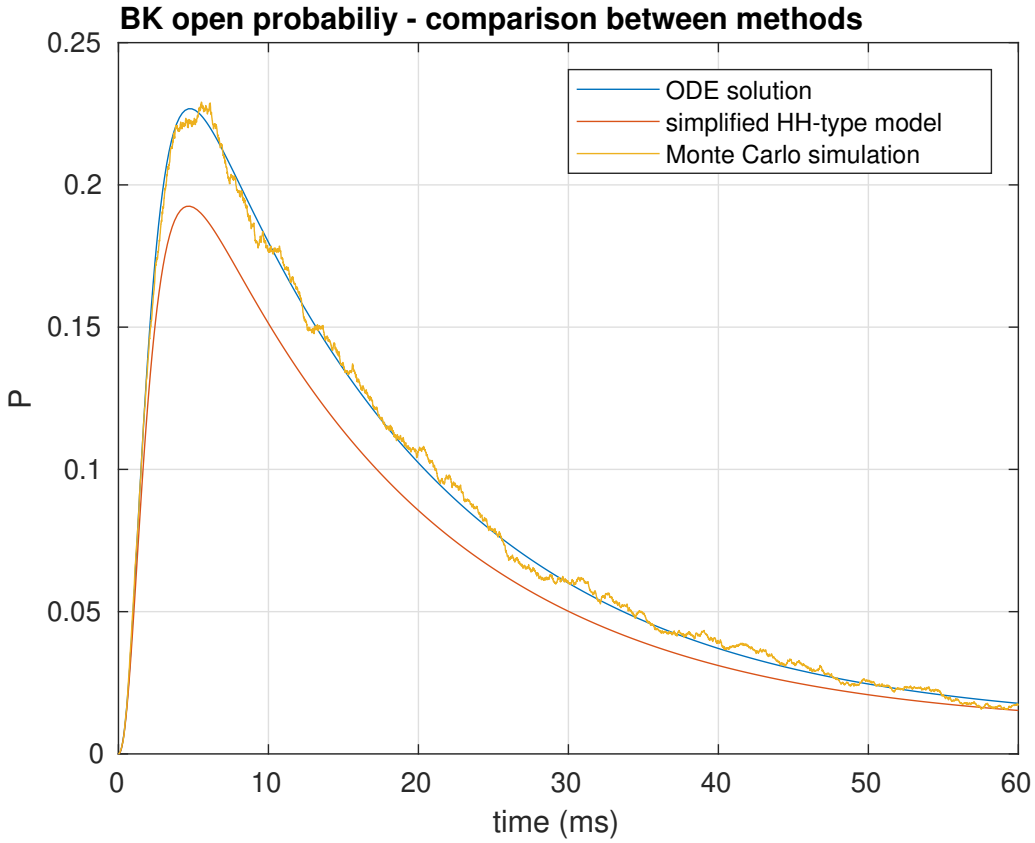

Figure 3.9: *BK open probability as function of time. Comparison between the methods presented: Monte Carlo simulation of the* 18*-state Markov chain, complete ODE system for the Markov chain and simplified ODE system obtained through the time scale analysis. We notice that, as it is in [1], the simplified ODE system constitutes a good approximation of the complete system.*

The result we are most interested in is the evolution of the BK open probability over time, that is shown in figure 3.9. The plot reports the comparison between the three methods that were tested. It is worth noticing that the evolution obtained from the simplified system of 8 equations (eq. 3.2-3.2, 3.2 and 3.2) approximate well the functions given by the Monte Carlo simulation of the Markov chain and by the complete system of 18 ODEs for the state probabilities, as it happens in the case with fixed distance between the channels ([1]). This means that the complications brought by the introduction of the CaV diffusion do not prevent us from finding a more manageable set of differential equations that is equally capable of describing the dynamics of the system.
Another interesting observation can be made comparing figure 3.9 to 3.7. We note that the 18-state Markov chain, defined for the interaction between the channels on the grid, actually reproduces the same BK open probability obtained from the Monte Carlo simulation presented in chapter 2, but it requires an extremely smaller computational cost.

In figure 3.10 we see the same kind of comparison between methods for the CaV open probability in time. This plot is virtually identical to the analogue one presented in [1], because the CaV activity is non affected by its diffusion on the cell membrane. This fact is evident also from figure 3.11, where it is possible to notice how the CaV activation variable obtained through the simplyfied ODE system reproduces the same dependance on the voltage as the CaV activation variable found in ([1]) for the model at fixed distance.
Figure 3.12 shows how the $m_{BK}i_{\infty}$ combine to give the steady state for the global activation variable of the potassium channel. This steady state, in blue in the plot, exhibits the same dependance on the voltage as the $m_{BK\infty}$ in ([1]), except for the fact that it is a bit lower, as a

consequence of the introduction of the CaV movement.

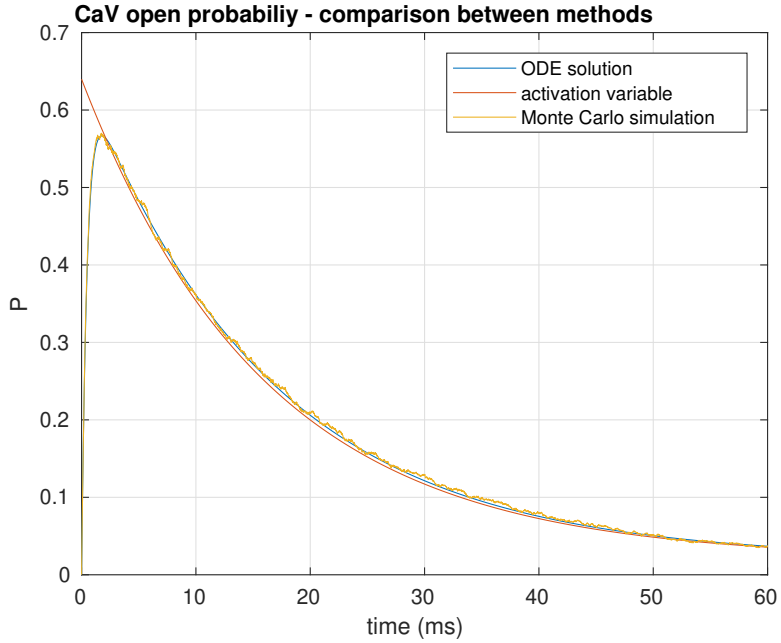

Figure 3.10: *CaV open probability as function of time. Comparison between methods: Monte Carlo simulation of the 9-state Markov chain for the CaV channel, complete ODE system for the Markov chain and simplified ODE system obtained through the time scale analysis. The plot reproduces the correspondent results in [1], validating the assumption that the CaV diffusion and its dynamics between states are independent processes.*

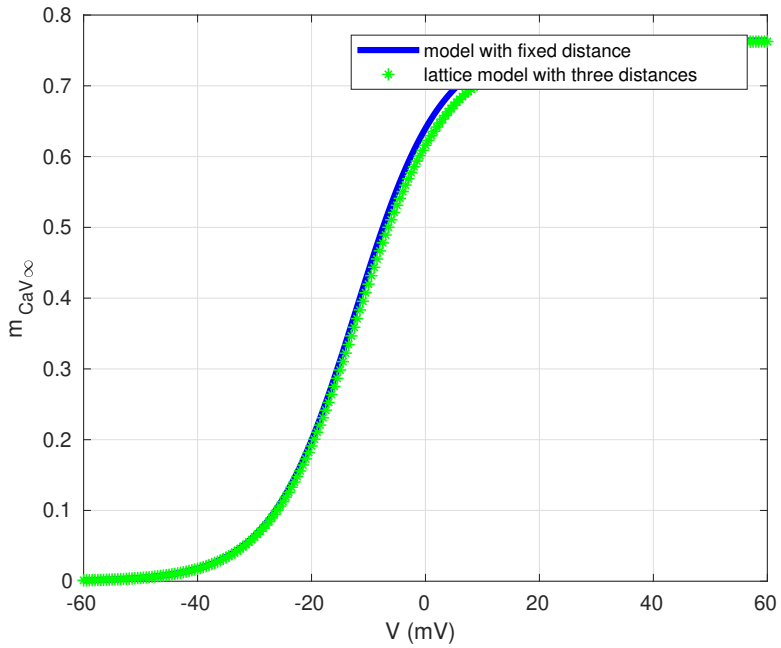

Figure 3.11: *Steady-state activation function for the CaV channel. Comparison between the results found in [1] for the model with fixed distance between the CaV and the BK (blue) and our results (green), obtained from the grid model with the three distances. The plot shows that our equations reproduce the CaV dynamics correctly.*

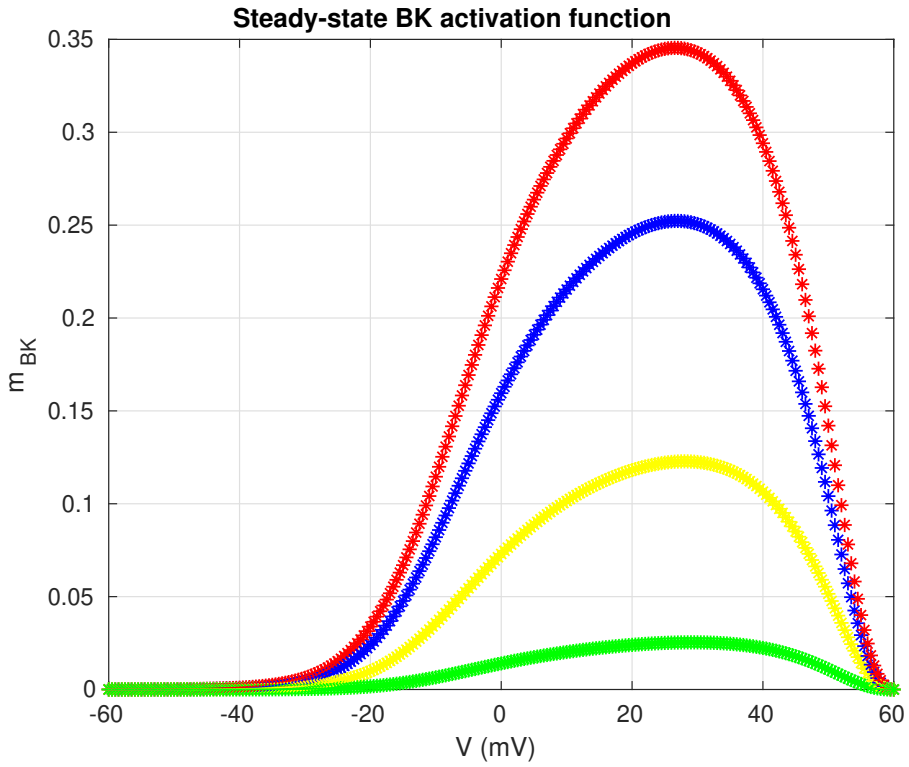

Figure 3.12: *Steady-state activation function for the BK channel. The different contributions are shown: the red line is $m_{BK\infty}1$, the yellow line is $m_{BK\infty}2$, the green line is $m_{BK\infty}3$ and the blue line is the weighted sum of these three functions, with weights equal to the steady-state probabilities of the CaV channel being at distance r_1, r_2 or r_3.*

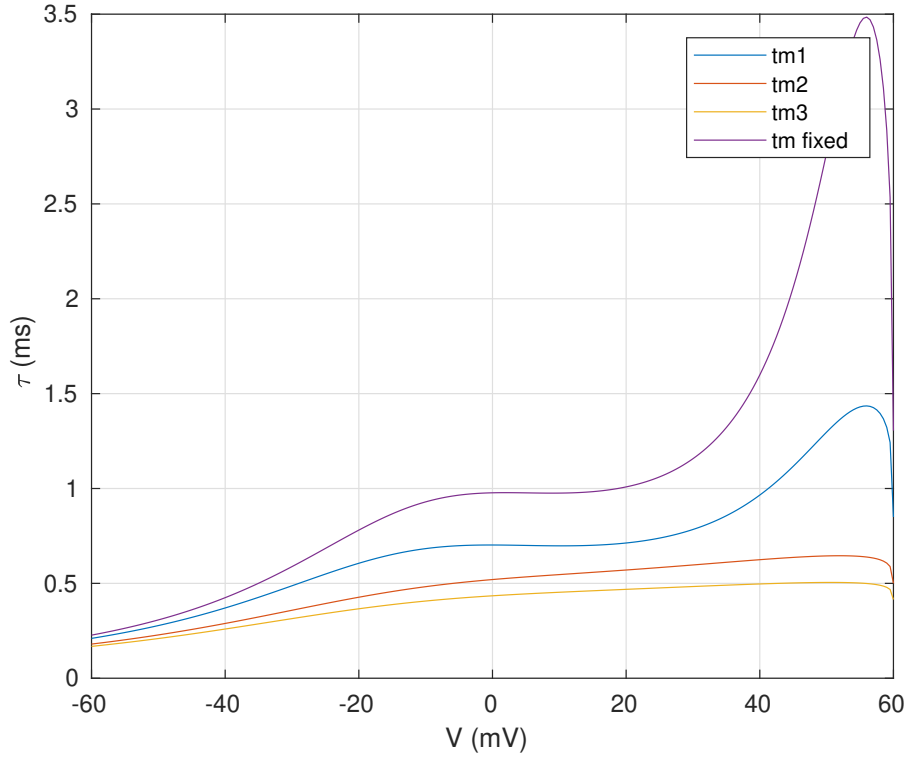

Figure 3.13: *Time constants for the BK activation functions $m_{BK}i_\infty$.*

Chapter 4

Conclusions

In chapter 2 we presented a Monte Carlo simulation of the interaction between the CaV channel and the BK channel that included the CaV diffusion around the BK. This simulation enabled us to obtain an estimate of the probability of complex formation, that appears to be quite small. However, the most interesting, and non-obvious, result of this section is offered by the study of the complex contribution to the BK open probability in time. We found that the BK channel is actually activated by a CaV to which is bonded only about 50% of the times. This result was not immediately predictable since the BK activation rate in presence of an open CaV exhibits a steep decreased as soon as the CaV channel moves away from the distance typical of the bond. But besides this, we know that, when the channels form the complex, the CaV movement is limited by the bond with the BK, which holds the CaV close for a certain amount of time. This residence time is $\approx 2\ ms$, that is two order or magnitude bigger than the time step over which we simulate the channel dynamics between its states, meaning the bonded CaV should have many opportunities to open and activate the BK in this conditions.
The Markov chain model devised in chapter 3 constitutes an extension of the one implemented in ([1]). Thanks to the results obtained in chapter 2, we are able to define the limits of this model and to estimate the quality of the approximation we make considering a grid with only three distances from the BK. The Monte Carlo simulation of the stochastic gating of the channels shows good accordance with the complete system of ODEs, which describes the state probabilities evolution over time. In particular it is evident that the introduction of the CaV diffusion brings much complications in the ODE system, keeping us from obtaining simple expressions for the activation variables that could offer a more significant insight on the role of the different processes. However, we were able to provide a reduced system of ODEs.
Even if the model shows aspects of consistency, we can not say if it brings an actual improvement respect to the model for the complex, implemented with the CaV at fixed distance from the BK, because we could not find appropriate experimental data to test the results. The next natural step, if one would want to continue this work, would be certainly to devise an approach to test these results.

References

[1] F. Montefusco et al. "Concise whole-cell modeling of $BK_{Ca} - CaV$ activity controlled by local coupling and stoichiometry". In: *Biophysical Journal* 112 (2017).

[2] H. Berkefeld, B. Fakler, and U. Schulte. "Ca^{2+}-activated K^+ channels: from protein complexes to function". In: *Physiological Review* 90 (2010).

[3] H. Berkefeld et al. "$BK_{Ca} - CaV$ channel complexes mediate rapid and localized Ca^{2+}-activated K^+ signaling". In: *Science* 314 (2006).

[4] D.H Cox. "Modeling a Ca^{2+} channel/BK_{Ca} channel complex at the single-complex level". In: *Biophysical Journal* 107 (2014).

[5] A.L. Hodgkin and A.F Huxley. "A quantitative description of membrane current and its application to conduction and excitation in nerve". In: *J. Physiol.* 117 (1952).

[6] B. Hille. "Ion channels of excitable membranes". In: (2001).

[7] K. Jacobson, L. Ping, and B.C. Lagerholm B.C. "The lateral organization and mobility of plasma membrane components". In: *Cell* 177 (2019).

[8] N.R Gandasi et al. "Ca^{2+} clustering with insulin-containing granules is disturbed in type 2 diabetes". In: *The journal of clinical investigation* 127.6 (2017).

[9] E. Neher. "Usefulness and limitations of linear buffer approximations to the understanding of Ca^{2+} signals". In: *Cell Calcium* 24 ().